Dynamic scaling of the island-size distribution and percolation in a model of submonolayer molecular-beam epitaxy

Jacques G. Amar and Fereydoon Family
Department of Physics, Emory University, Atlanta, Georgia 30322

Pui-Man Lam
Department of Physics, Emory University, Atlanta, Georgia 30322
*and Department of Physics, Southern University, Baton Rouge, Louisiana 70813**
(Received 20 January 1994; revised manuscript received 1 April 1994)

The results of a detailed study of the evolution, scaling, and percolation of islands in a model of submonolayer molecular-beam epitaxy appropriate for the case of dendritic island growth are presented. The scaling of the island density, monomer density, island-size distribution, structure factor, and pair-correlation function are studied as a function of the coverage θ and the ratio $R=D/F$ of the diffusion rate D to the deposition rate F. Our results span the full range of coverage starting from very low coverage all the way through the coalescence and percolation regimes. For small coverages the islands are fractal while at higher coverages they become compact, similar to what has been observed in Au/Ru(0001). For large R, four distinct scaling regimes are found: a low-coverage nucleation regime, an intermediate-coverage regime, an aggregation regime in which the island density remains constant, and a coalescence and percolation regime. The scaling behavior in the first three regimes is compared with results obtained using a generalized rate-equation approach. An anomalous fractal scaling form for the structure factor in the aggregation regime is also derived. The dependence of the percolation threshold on R is also studied and found to show interesting nonmonotonic behavior.

I. INTRODUCTION

The fundamental physical processes in the growth of thin films by deposition techniques, such as molecular-beam epitaxy (MBE), involve nucleation, aggregation, and coalescence of islands on a two-dimensional substrate.[1-3] This leads to the formation of a distribution of islands of various sizes and morphologies which grow and coalesce with time. The classic work of Smoluchowski[4,5] on the rate equation and more recent work on the development of dynamic scaling ideas,[6-8] have provided powerful tools for the analysis and understanding of growth and aggregation processes in terms of the evolution of the cluster-size distribution. In particular, dynamic scaling of the cluster-size distribution as well as the Smoluchowski rate-equation approach have been applied to detailed studies of aggregation processes[6,9,10-13] as well as thin-film growth.[8,14-17]

With the recent development of analytical tools such as the scanning tunneling microscope and high-resolution diffraction and scattering techniques which can effectively probe the morphology and the growth of microstructures at the surface, the study of submonolayer evolution in MBE and other deposition techniques has received considerable attention (see Ref. 3 and references therein). In particular, using various experimental techniques it is now possible to study the submonolayer island morphology, density, and size distribution in a variety of systems ranging from homoepitaxial systems such as Fe/Fe(100),[18] Ni/Ni(100),[19] Si/Si(100),[20] and Cu/Cu(100),[21] to heteroepitaxial systems such as Pb/Cu(001),[22] Au/Ru(0001),[23] and Ag/Si(111).[24] From these measurements, other important quantities may be determined. In particular, such parameters as the adatom diffusion constant $D=D_0\exp(-E_a/kT)$ and the activation energy E_a for surface diffusion can be determined experimentally by measuring the scaling of the island density N as a function of temperature and deposition rate F at low coverage.[20,21] For example, the exponent χ governing the scaling of the island density N at fixed coverage θ, $N\sim(D/F)^{-\chi}$ may be determined experimentally by studying the variation of N with the deposition rate F. Once χ is known, the activation energy E_a for diffusion may be determined from the scaling of the island density as a function of temperature. If the constant $C_1=N(D/F)^{\chi}$ is known, then the prefactor D_0 in the diffusion constant $D=D_0\exp(-E_a/kT)$ can be determined. Thus the knowledge of the scaling behavior of the island density and size distribution for simple models of island formation both in the very-early-time and the aggregation regime may enable the determination of important physical quantities in epitaxial growth.

Recently, these techniques have been used to study island morphology and evolution in the submonolayer regime, and dendritic island growth has been observed in a variety of systems. One example is the experimental study of the deposition of Au on Ru(0001) at room temperature.[23] In these experiments, the morphology of the islands was studied using scanning tunneling microscopy, and they were found to be fractal at low coverages $\theta\leq 0.3$, with a fractal dimension $d_f\simeq 1.7$ corresponding to that of diffusion-limited aggregation (DLA), while for

higher coverages they were seen to become compact. Two other examples are Ag/Ni(100) (Ref. 25) and Ag/Au(111),[26] in which dendritic step decoration has been observed. Dendritic island growth has also been observed near $T=200$ K for Pt/Pt(111).[27,28] This is consistent with the prediction[29,30] that for homoepitaxy on fcc(111) surfaces, island relaxation due to edge diffusion is inhibited. Consistent with this scenario, recent theoretical calculations using density-functional theory[31] predict fractal growth for Al/Al(111) for 25 K $<T<$ 155 K. Thus one may conclude that dendritic island growth may occur in a wide variety of systems including both homoepitaxy and heteroepitaxy.

In this paper we investigate the evolution, growth, and scaling of islands in a model of submonolayer MBE appropriate for the case of dendritic island growth over the full range of coverage, starting from very low coverage ($\theta \simeq 10^{-5}$) all the way through the coalescence and percolation regimes.[16] In our model, monomers are deposited randomly on a two-dimensional lattice, and allowed to diffuse with nearest-neighbor hops. To simulate low-temperature MBE and/or dendritic island growth, we assume that whenever an adatom encounters another adatom as its nearest neighbor, both atoms are "frozen" (stop diffusing) and form a stable two-atom cluster or island. Similarly, when a diffusing adatom encounters an existing island, it is attached to the island cluster and becomes immobile. An adatom deposited on top of an existing island or monomer (second-layer growth) also diffuses, and if it encounters another adatom or island on the same adlayer it is frozen. However, if it first diffuses over the edge of the island to the layer below (there is no barrier to going down a step) it is added to the island. Thus for large D/F (which as we shall see corresponds to the scaling regime) there is a negligible amount of second-layer growth (at least below percolation) since the second-layer atoms quickly diffuse to the edge of an island and down to the first layer where they join the cluster.

The paper is organized as follows. In Sec. II we present an introduction to the scaling theory for the island-size distribution and define the relevant exponents which characterize the scaling behavior of the island density, monomer density, and the island-size distribution with coverage θ and the ratio D/F. In Sec. III the Smoluchowski kinetic equation for the evolution of the island-size distribution and the corresponding rate equations for the island density and monomer density are discussed. We introduce our model and describe our simulations in Sec. IV. In Sec. V, we present our results and compare them with the predictions of the generalized rate equations discussed in Sec. III. Finally, we summarize our results in Sec. VI.

II. SCALING THEORY

The fundamental quantity in the kinetic description of island growth is the island-size distribution function $N_s(t)$, which gives the density (per site) of islands of size s (where s is the number of atoms or particles in the island) at time t. Since the coverage $\theta=Ft$ is often more convenient for comparison with experiments, we express the time dependence of the island-size distribution and its moments in terms of θ. Defining the total island density N (excluding monomers) and the coverage θ by

$$N=\sum_{s\geq 2} N_s(\theta) \quad \text{and} \quad \theta=\sum_{s\geq 1} sN_s \ , \tag{1}$$

then the average island size S can be written in terms of the zeroth and first moments as

$$S=\frac{\sum_{s\geq 2} sN_s(\theta)}{\sum_{s\geq 2} N_s(\theta)}=\frac{(\theta-N_1)}{N} \ , \tag{2}$$

where N_1 is the monomer density.

According to the dynamic scaling assumption[6-8,14] there exists only one characteristic size in the problem which is the mean island size $S(\theta)$ defined in (2). This implies that $N_s(\theta)$ scales with $S(\theta)$, and one may write generally $N_s(\theta)=A(S,\theta)f(s/S)$, where $f(u)$ is a scaling function for the island-size distribution. Using the definition of θ and the scaling form for the island-size distribution, we can write, $\theta=\sum_{s\geq 1} sN_s(\theta) = A(S,\theta)S^2\int_0^\infty f(u)u\,du$, which implies $A(S,\theta)\sim\theta/S^2$. Taking $A(S,\theta)=\theta/S^2$, one may write the general scaling form

$$N_s(\theta)=\theta S^{-2}f(s/S) \quad (s\geq 2) \ , \tag{3}$$

where the scaling function $f(u)$ satisfies $\int_0^\infty f(u)u\,du=1$, and $f(u)\sim u^\omega$ for $u\ll 1$.

We now assume that at late time (and for large R), the average cluster size S scales as

$$S\sim R^\chi\theta^z \ , \tag{4}$$

where $R=D/F$ is the ratio of the diffusion rate D to the deposition rate F. Equation (3) may then be rewritten in the form

$$N_s(\theta)=R^{-2\chi}\theta^{1-2z}g_1\left[\frac{s}{R^\chi\theta^z}\right] \ , \tag{5}$$

where $g_1(u)=(1/c^2)f(u/c)$, where $c=S/(R^\chi\theta^z)$. Alternatively, one may rewrite this in the form

$$N_s(\theta)=s^{-\tau}R^{-\chi/z}g_2\left[\frac{s}{R^\chi\theta^z}\right] \ , \tag{6}$$

where $\tau=2-1/z$ and $g_2(u)=u^\tau g_1(u)$.

At late time, one expects the walker density N_1 to be much smaller than the coverage θ, so that in the scaling regime $N_1\ll\theta$ and $S\simeq\theta/N$. This implies the scaling relation for the total island density,

$$N\simeq\theta/S\sim R^{-\chi}\theta^{1-z} \ . \tag{7}$$

Thus we have obtained scaling relations for $N(\theta)$, $S(\theta)$, and $N_s(\theta)$ as functions of R and θ with two independent exponents χ and z. Comparison with Eqs. (1) and (3) implies that the scaling function, in addition to satisfying $\int_0^\infty f(u)u\,du=1$, also satisfies the relation $\int_0^\infty f(u)du=1$.

In addition to the scaling relations above for the island

density and size distribution, we may also define scaling exponents for the monomer density N_1 of the form

$$N_1 \sim R^{-\gamma}\theta^{-\nu} . \tag{8}$$

If we assume that the scaling form for $N_s(\theta)$ also holds for N_1, then from Eqs. (3) and (5) we obtain

$$\gamma=(\omega+2)\chi , \quad \nu=(\omega+2)z-1 . \tag{9}$$

We note that for the point-island model in $d=2$,[33,34] Eq. (9) holds since for this model $\omega=0$, $z=\gamma=\frac{2}{3}$, and $\nu=\chi=\frac{1}{3}$. However, Eq. (9) does not generally hold for more realistic models, since the monomer density N_1 may in general scale differently from the island density $N_s(\theta)$ for $s \geq 2$.

III. RATE-EQUATION APPROACH

The traditional method for studying the kinetics of cluster growth processes is based on the theoretical approach developed by Smoluchowski,[4,5] who wrote an equation for the evolution of the cluster-size distribution using a mean-field argument which neglects fluctuations and geometry. For the case of growth in which only monomers diffuse, one can write down a simple set of equations[32-38] governing the density of monomers N_1 and the density $N_s(t)$ of islands of size s at time t. Ignoring dissociation, one has generally,

$$\frac{dN_1}{dt}=F-K_1N_1^2-N_1\sum_{s\geq 2}K_sN_s , \tag{10a}$$

$$\frac{dN_s}{dt}=N_1(K_{s-1}N_{s-1}-K_sN_s) \quad (s>1) , \tag{10b}$$

where F is the rate of deposition of atoms (in units of atoms deposited per site per unit time) and K_s governs the rate of attachment of adatoms (monomers) to islands of size s. The exponents are usually determined by substituting the scaling forms (6) and (8) into (10), and by assuming a general[9,10,12,13] form $K_s \sim Ds^p$ for the dependence of the rate constant on cluster size, where D is the diffusion rate of single adatoms (in units of hops per unit time). Ignoring the proportionality factor (which may be different for K_s, $s \geq 2$, and K_1) since it does not affect the scaling behavior, and dividing by the deposition rate F, Eq. (10) may be rewritten,

$$\frac{dN_1}{d\theta}=1-RN_1^2-RN_1\sum_{s\geq 2}s^pN_s , \tag{11a}$$

$$\frac{dN_s}{d\theta}=N_1R[(s-1)^pN_{s-1}-s^pN_s] \quad (s>1) , \tag{11b}$$

where $R=D/F$ and $\theta=Ft$ is the coverage (number of atoms deposited per site). Rewriting in terms of the scaled variables $\hat{\theta}=R^{1/2}\theta$ and $\hat{N}_s=R^{1/2}N_s$, Eq. (11) becomes

$$\frac{d\hat{N}_1}{d\hat{\theta}}=1-\hat{N}_1^2-\hat{N}_1\sum_{s\geq 2}s^p\hat{N}_s , \tag{12a}$$

$$\frac{d\hat{N}_s}{d\hat{\theta}}=\hat{N}_1[(s-1)^p\hat{N}_{s-1}-s^p\hat{N}_s] \quad (s>1) . \tag{12b}$$

For the point-island model, the islands have zero size,[33,34] and one has $K_s \sim D$ ($p=0$). In this case Eq. (12) becomes

$$\frac{d\hat{N}_1}{d\hat{\theta}}=1-\hat{N}_1^2-\hat{N}_1\sum_{s\geq 2}\hat{N}_s \tag{13a}$$

$$\frac{d\hat{N}_s}{d\hat{\theta}}=\hat{N}_1(\hat{N}_{s-1}-\hat{N}_s) \quad (s>1) . \tag{13b}$$

Defining the total scaled island density as $\hat{N}=\sum_{s\geq 2}\hat{N}_s$, and summing Eq. (13b) over s for $s \geq 2$, one obtains the point-island rate equations

$$\frac{d\hat{N}_1}{d\hat{\theta}}=1-\hat{N}_1^2-\hat{N}_1\hat{N} , \tag{14a}$$

$$\frac{d\hat{N}}{d\hat{\theta}}=\hat{N}_1^2 . \tag{14b}$$

The solution of these equations is as follows. In the early-time low-coverage regime $\hat{\theta} \ll 1$ ($\theta \ll R^{-1/2}$) in which islands are still nucleating and the island density N is much less than the monomer density ($\hat{N} \ll \hat{N}_1$) which is very small, the last two terms on the right of (14a) may be neglected, so that one has

$$\hat{N}_1=\hat{\theta} , \quad \hat{N} \sim \hat{\theta}^3 , \tag{15}$$

which implies $N_1=\theta$ and $N \sim R\theta^3$. (Taking higher order corrections into account, one has $\hat{N}_1=\hat{\theta}-\hat{\theta}^5/15$ and $\hat{N}=\hat{\theta}^3-2\hat{\theta}^7/105$.) At late times ($\hat{\theta} \gg 1$), the island density will increase to the point where the last two terms on the right of Eq. (14a) become important, leading to the decrease of the monomer density so that $\hat{N}_1 \ll \hat{N}$. Equating these two terms (neglecting the middle term since $\hat{N}_1 \ll \hat{N}$) and using Eq. (14b), in the asymptotic regime $\hat{\theta} \gg 1$ one obtains

$$\hat{N} \sim \hat{\theta}^{1/3} , \quad \hat{N}_1 \sim \hat{\theta}^{-1/3} . \tag{16}$$

Thus for $\theta \gg R^{-1/2}$ one has $N \sim R^{-1/3}\theta^{1/3}$, $N_1 \sim R^{-2/3}\theta^{-1/3}$, and $S \simeq \theta/N \sim R^{1/3}\theta^{2/3}$, which implies that $\nu=\chi=\frac{1}{3}$ and $\gamma=z=\frac{2}{3}$ for the point-island model.

For realistic models in which the islands have finite size one expects $p \neq 0$. Blackman and Wilding[32] have suggested that the rate of capture of monomers by an island of size s is proportional to the linear dimension (cross section) of the island as well as the diffusion constant D. For compact islands in two dimensions this implies $p=\frac{1}{2}$, while for fractal islands it implies $p=1/d_f$, where d_f is the fractal dimension of the island. They determined the exponents z, ν, and $\tau=2-1/z$ for general p using an analysis of the moments $M_n=\sum_s s^nN_s$ based on Eq. (10) with $K_s \sim s^p$. In addition, they numerically integrated Eq. (10). Here we proceed somewhat differently by using a heuristic argument to modify the scaled rate equation for the total island density N, but our results for z, ν, and τ are the same. However, in addition to determining these exponents, we also determine the exponents χ and γ governing the R dependence of N and N_1.

First we note that for $p \neq 0$ the rate R_{att} at which ada-

toms are attached to existing islands is no longer written as $R_{att} \sim DN_1 N$ but rather as $R_{att} \sim DN_1 \sum_{s \geq 2} N_s s^p$, which we may approximate in the scaling regime as $R_{att} \sim DN_1 NS^p$, where S is the average number of atoms in an island. Thus the rate equation (10a) becomes, $dN_1/dt \simeq F - DN_1^2 - DN_1 NS^p$. In the late-time regime in which we are interested, one has $N_1 \ll \theta$, so that $S = (\theta - N_1)/N \simeq \theta/N$. Thus the rate equations in this regime become

$$\frac{dN_1}{dt} = F - DN_1^2 - DN_1 \theta^p N^{1-p} , \tag{17a}$$

$$\frac{dN}{dt} = DN_1^2 . \tag{17b}$$

Dividing by F and rewriting in terms of the scaled variables $\hat{\theta} = (D/F)^{1/2}\theta$, $\hat{N} = (D/F)^{1/2}N$, and $\hat{N}_1 = (D/F)^{1/2}N_1$, we obtain

$$\frac{d\hat{N}_1}{d\hat{\theta}} = 1 - \hat{N}_1^2 - \hat{N}_1 \hat{N}^{1-p} \hat{\theta}^p , \tag{18a}$$

$$\frac{d\hat{N}}{d\hat{\theta}} = \hat{N}_1^2 . \tag{18b}$$

For $p \leq 1/2$ we assume power-law solutions of the form $\hat{N} \sim \hat{\theta}^{1-z}$ and $\hat{N}_1 \sim \hat{\theta}^{-\nu}$ (see Sec. II). In the scaling regime in which $\hat{N} \gg \hat{N}_1$ and $d\hat{N}_1/d\hat{\theta}$, $\hat{N}_1 \ll 1$, we can ignore the second term on the right of Eq. 18(a) and equate the first and third terms, i.e., $1 = \hat{N}_1 \hat{N}^{1-p} \hat{\theta}^p$. Using the latter equality as well as Eq. 18(b), and replacing the scaled variables, one obtains

$$z = 2/(3-2p) , \quad \nu = z/2 , \quad \chi = z/2 , \quad \gamma = \tfrac{1}{2} + z/4 \quad (p < \tfrac{1}{2}) . \tag{19a}$$

Thus for $p < \frac{1}{2}$,

$$N \sim R^{-z/2} \theta^{1-z} , \quad N_1 \sim R^{-(1/2+z/4)} \theta^{-z/2} \quad (p < \tfrac{1}{2}) . \tag{19b}$$

For the special case $p = \frac{1}{2}$, one has $z = 1$, and there are logarithmic corrections,

$$N \sim R^{-1/2} \ln(\theta), \quad N_1 \sim R^{-3/4} \theta^{-1/2} \quad (p = \tfrac{1}{2}) , \tag{20a}$$

which implies that

$$z = 1 , \quad \nu = \tfrac{1}{2} , \quad \chi = \tfrac{1}{2} , \quad \gamma = \tfrac{3}{4} \quad (p = \tfrac{1}{2}) . \tag{20b}$$

For the case $p > \frac{1}{2}$ we assume $\hat{N} = \text{const} - a/\hat{\theta}^q$, which implies $z = 1$ and again $\hat{N}_1 \sim \hat{\theta}^{-\nu}$. Substituting into Eq. (18) as before, this implies

$$z = 1, \quad q = 2p - 1 , \quad \nu = p , \quad \chi = \tfrac{1}{2} , \quad \gamma = (1+p)/2 \quad (p > \tfrac{1}{2}) . \tag{21a}$$

In terms of the unscaled variables,

$$N \sim R^{-1/2}(1 - aR^{-q/2}\theta^{-q}) , \quad N_1 \sim R^{-(1+p)/2} \theta^{-p} \quad (p > \tfrac{1}{2}) . \tag{21b}$$

For the case of fractal islands with $d_f = 1.7$, we have $p = 1/d_f \simeq 0.58$, which implies $\nu \simeq 0.58$, $\gamma \simeq 0.79$, and $q \simeq 0.16$.[39]

IV. MODEL AND SIMULATIONS

In our model, adatoms (monomers) are deposited randomly on a square lattice with deposition rate F (in units of atoms per site per unit time), and then diffuse with diffusion rate D (nearest-neighbor hops per adatom per unit time). An adatom deposited on top of an existing island or monomer (second-layer growth) also diffuses with diffusion rate D. When an adatom encounters another adatom as its nearest neighbor, both atoms are frozen (stop diffusing) and form a stable two-atom cluster or island. Similarly, when a diffusing adatom encounters an existing island, it is attached to the island cluster and becomes immobile. At each stage, either a deposition step (consisting of the deposition of one adatom at a randomly chosen site) or a diffusion step (consisting of the diffusion by one nearest-neighbor lattice site of a randomly chosen walker) is carried out. In order to properly keep track of the competing rates of diffusion and deposition, the deposition step was carried out with probability $p_F = 1/[1 + N_1(D/F)]$, where N_1 is the monomer density (per site). Similarly, the diffusion step was carried out with probability $p_D = 1 - p_F = N_1(D/F)/[1 + N_1(D/F)]$.[40,41] A list of all monomers or walkers was continually updated, and if a monomer encountered another particle (i.e., another monomer or part of a cluster) as its nearest neighbor, then that monomer was added to the cluster and removed from the walker list.

We note that in our model there is no additional barrier or activation energy for jumping down a step (Schwoebel effect[42]). This is consistent with the observation for island growth of Au on Ru(0001) that Au atoms can easily diffuse over first-layer island steps to condense at their edge in the bottom layer.[23] Thus the Schwoebel effect (barrier) is not expected to be very large in this system. We also note that while the magnitude and sign of the Schwoebel barrier effect is expected to vary from system to system, there are a number of other systems [such as Al/Al(111) (Ref. 31)] for which the barrier is believed to be negligible compared to the diffusion activation energy over a large range of temperatures. Even for systems for which the Schwoebel barrier is more significant, it has been shown[43] that for small islands, as well as for islands which have small features due to lack of relaxation (such as fractal islands), that the energy of condensation upon surface impingement may be sufficient to lead to incorporation of the adatom directly into the cluster, thus overcoming the Schwoebel barrier in these systems. Such an assumption has been made in recent simulations by Smilauer, Wilby, and Vvedensky,[44] in which it was used to explain the reentrance of layer-by-layer growth with decreasing temperature in deposition of Pt/Pt(111).[45]

Our simulations typically involved system sizes ($L \times L$) ranging from $L = 400$ to 1024, with periodic boundary conditions. (Smaller system sizes were also used to obtain snapshots of the island morphology.) Averages were taken over 50–200 runs, and simulations were conducted for different values of the ratio D/F ranging from 10 to 10^9.

In our simulations, we kept track of the monomer density N_1, the total density N of first-layer islands, and the first-layer island-size distribution N_s, all as a function of the coverage θ from very low coverage ($\theta \simeq 10^{-5}$) to a coverage $\theta = 1$. In addition, we monitored the number of nucleation events in order to determine directly the rate of coalescence of islands as a function of coverage. We also calculated the normalized circularly averaged first-layer density-density pair-correlation function $G(r) = (\theta - \theta^2)^{-1} \langle \bar{n}(0)\bar{n}(r) \rangle_c$, where $\bar{n}(r) = n(r) - \theta$ and the brackets denote a circular average as well as an average over runs. Here the density $n(r) = 1$ at a site r at which there is an adlayer atom, and 0 otherwise. Finally, we also calculated the circularly averaged structure factor $S(k) = \langle (1/L^2) | \sum_{\mathbf{r}} \bar{n}(\mathbf{r}) e^{i\mathbf{k}\cdot\mathbf{r}} |^2 \rangle_c = \langle \sum_{\mathbf{r}} \langle \bar{n}(\mathbf{0})\bar{n}(\mathbf{r}) \rangle e^{-i\mathbf{k}\cdot\mathbf{r}} \rangle_c$.

In order to study the morphology of the islands, we also calculated the radius of gyration of the clusters R_G and studied the dependence of R_G on the island size s. Assuming that $R_G \sim s^{1/d_f}$, we calculated the fractal dimension d_f of the islands as a function of the ratio $R = D/F$ at several values of the coverage θ. We also determined the percolation threshold (i.e., the coverage θ_p at which a single island first percolated through the lattice) as well as the first-layer coverage at percolation θ_{1p} as a function of $R = D/F$.

V. RESULTS

Figure 1 shows an overview of our results for the variation of the island density and monomer density as a function of coverage for a given value of $R = D/F$. As can be seen from Fig. 1, we find that the dynamical behavior of both N and N_1 is divided into four distinct regimes: a low-coverage nucleation regime (L), an intermediate-coverage regime (I), an aggregation regime (A), and a coalescence and percolation regime (C). In the low-coverage nucleation regime, the monomer density is much larger than the island density which is increasing due to the nucleation of new islands. In the intermediate-coverage regime the island density is larger than the monomer density, so that the monomer density is decreasing while the island density continues to increase. In the aggregation regime, the island density and size have become sufficiently large that every adatom deposited lands either near or on top of an island. As a result the island density remains essentially constant while the monomer density is sharply decreasing. Finally, in the coalescence regime, the islands begin to join together and percolate so that eventually second-layer growth occurs and the monomer density increases.

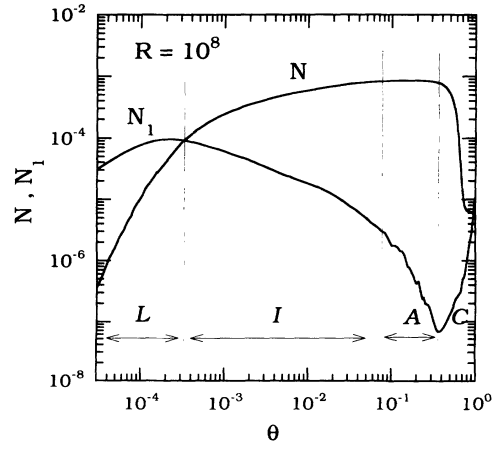

FIG. 1. Log-log plot of unscaled island density N and monomer density N_1 as a function of coverage θ for $R = 10^8$ showing the four scaling regimes.

Figure 2 shows pictures which give an overview of the typical island morphology and distribution for three different values of D/F ($D/F = 10^5$, 10^7, and 10^9) and for three different values of the coverage ($\theta = 0.1$, 0.3, and 0.7) corresponding to the very beginning of the aggregation regime ($\theta = 0.1$), the middle of the aggregation regime ($\theta = 0.3$), and the coalescence and percolation regime ($\theta = 0.7$). As can be seen from the pictures, for relatively low coverage the islands are fractal as is observed in a number of experiments,[23,25,27,28] while at higher coverage they become compact. We now discuss each of these scaling regimes in detail.

A. Low-coverage nucleation regime $\theta \ll R^{-1/2}$

The low-coverage regime has been studied previously for the point-island model by Bartelt and Evans[34] and also by Tang[33] in a model similar to ours. In this regime ($\hat{\theta} \ll 1$), the island density is much smaller than the monomer density, so that the probability of island growth is much smaller than the probability of nucleation. Therefore the average island size is very small and the point-island rate equations (14) are expected to be correct except for logarithmic corrections due to diffusion in two dimensions. In this regime, these equations [see Eq. (15)] imply $\hat{N}_1 \simeq \hat{\theta}$ and $\hat{N} \sim \hat{\theta}^3$, or $N_1 \simeq \theta$ and $N \sim R\theta^3$. Taking into account higher-order corrections (see Sec. III), one obtains $S = (\hat{\theta} - \hat{N}_1)/(\hat{N}) \sim \hat{\theta}^2 \ll 1$, so that for the ratio d/l (where d is a typical island diameter and l is the distance between islands), one obtains $d/l \sim (SN)^{1/2} \sim (R^{-1}\hat{\theta}^5)^{1/2} \ll 1$. Thus the point-island approximation is reasonable in this regime. However, since $d = 2$ is the critical dimension for diffusion-limited cluster growth, it is expected that there will be logarithmic corrections to the scaling behavior.[33]

Figure 3 shows scaling plots of our results for the monomer and island density using the form predicted by Eq. (15), with the addition of the approximate logarithmic correction factor $1/\sqrt{\ln(2Dt)} = 1/\sqrt{\ln(2R\theta)}$ proposed in Ref. 33. As can be seen, the scaled monomer density $N_1 R^{1/2}/[\ln(2R\theta)]^{1/2}$ as a function of the scaled coverage $\theta R^{1/2}/[\ln(2R\theta)]^{1/2}$ is independent of R, all the way up to and including the peak. Since the scaled coverage at the peak of the scaled monomer density in Fig. 3 is a constant (approximately 0.6), we can solve approximately for the coverage $\bar{\theta}_1$ at the peak of N_1 to obtain $\bar{\theta}_1 \simeq 0.4[\ln R/R]^{1/2}$. Also shown in Fig. 3 is the scaled island density $NR^{-1/2}$ versus $\theta R^{1/2}/[\ln(2R\theta)]^{1/2}$. This is different from Ref. 33, in which the logarithmic factor was included in both the scaled island density as well as the scaled monomer density. As can be seen in Fig. 3, we

find improved scaling for the island density data which now scales quite well for $\theta \ll R^{-1/2}$ and $R \geq 10^5$.

B. Intermediate-coverage regime ($R^{-1/2} \ll \theta \ll \theta_1$)

As the coverage increases, the monomer density N_1 peaks and begins to decrease, while the island density increases much more slowly than in the early-time nucleation regime. For $\theta \gg R^{-1/2}$ ($\hat{\theta} \gg 1$), the point-island rate equations (14) predict $\hat{N}_1 \sim \hat{\theta}^{-1/3}$ and $\hat{N} \sim \hat{\theta}^{1/3}$, which implies that $N_1 \sim R^{2/3}\theta^{-1/3}$ and $N \sim R^{1/3}\theta^{1/3}$. This also implies that $N_1/N = 1/\hat{\theta}^{2/3} \ll 1$, so that the average cluster size $S \simeq \theta/N = \hat{\theta}^{2/3} \gg 1$. Consequently in this regime the size of the islands becomes important, and

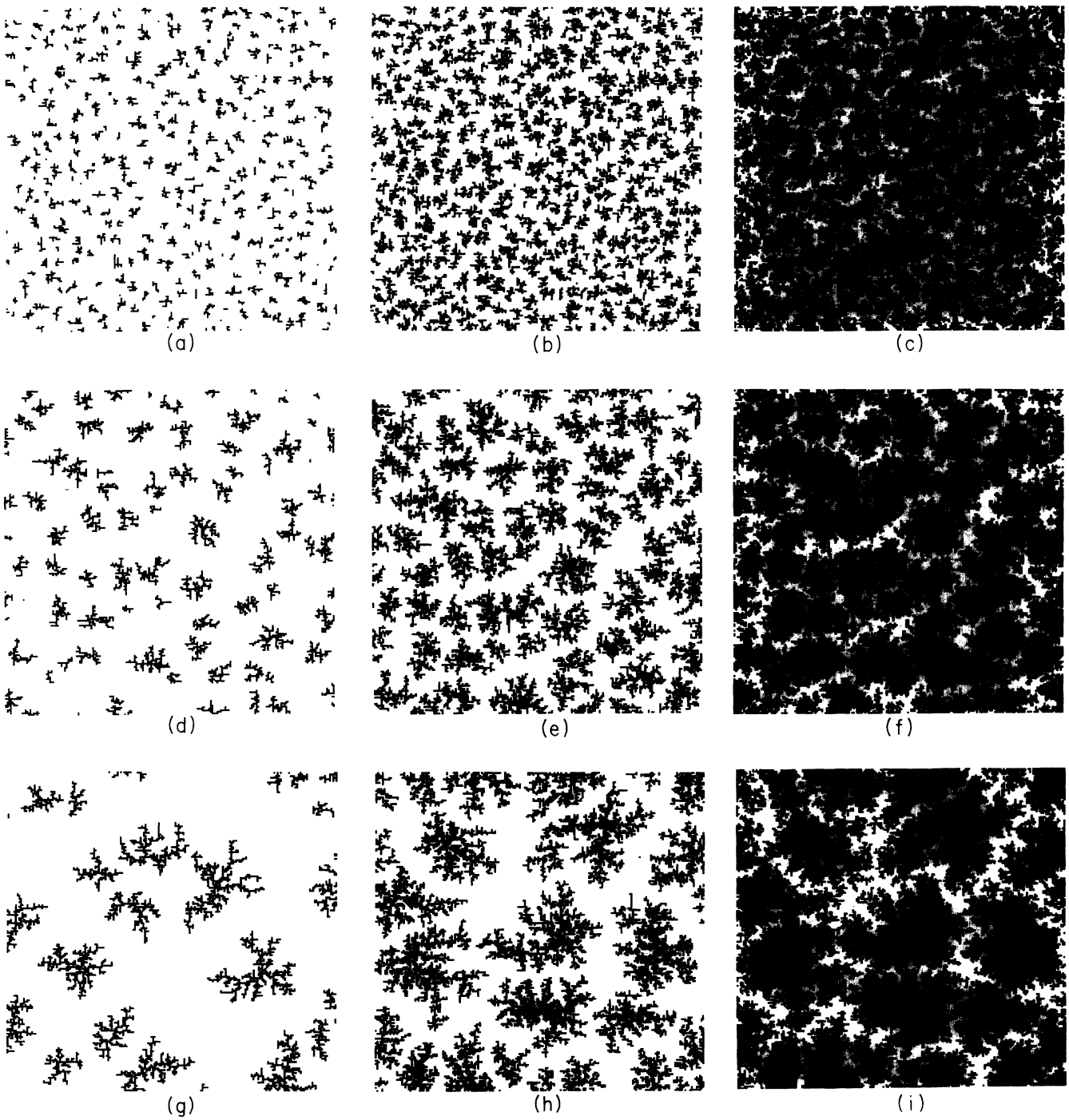

FIG. 2. Pictures of the island morphology ($L=200$) for three different values of R ($R=10^5$, 10^7, and 10^9) and three different coverages $\theta=0.1$, 0.3, and 0.7 in the beginning and middle of the aggregation regime, and in the coalescence regime. (a) $R=10^5$, $\theta=0.1$. (b) $R=10^5$, $\theta=0.3$. (c) $R=10^5$, $\theta=0.7$. (d) $R=10^7$, $\theta=0.1$. (e) $R=10^7$, $\theta=0.3$. (f) $R=10^7$, $\theta=0.7$. (g) $R=10^9$, $\theta=0.1$. (h) $R=10^9$, $\theta=0.3$. (i) $R=10^9$, $\theta=0.7$.

the point-island model and rate equations[34] must break down even for coverages low enough that deposition on top of islands and island coalescence may be neglected.

Figure 4 shows a log-log scaling plot of $N_1 R^{2/3}$ and $NR^{1/3}$ versus θ, which shows more clearly both the coverage dependence and the D/F dependence of the island density and monomer density in and beyond the intermediate-coverage regime. Surprisingly, in the intermediate-coverage regime the R dependence of the monomer density N_1 agrees reasonably well with the point-island prediction [see Eq. (16)] $\gamma=\frac{2}{3}$.[46] However, the dynamical behavior of the monomer density N_1 does not, since instead of decreasing as $N_1 \sim \theta^{-1/3}$ the monomer density varies as $N_1 \sim \theta^{-0.53}$, which implies $\nu \simeq \frac{1}{2}$ rather than $\nu=\frac{1}{3}$. Similarly, as shown in Fig. 4, over the same coverage range ($10^{-3}<\theta<0.02$) the curves of island density versus coverage for fixed R show strong curvature rather than a slope of $\frac{1}{3}$ as predicted by the point-island model. Similarly, for fixed coverage the density N does not scale as $N \sim R^{-\chi}$ with $\chi=\frac{1}{3}$, as predicted by the point island model.

Figure 5 shows a semilogarithmic plot of the island density in the intermediate-coverage regime as a function of coverage for three different values of R, indicating that in this regime the growth of the island density is essentially logarithmic, i.e., $N \sim \theta^{1-z} \sim A(R)\ln(\theta)$, which implies that $z=1$. We have also observed similar logarithmic behavior for the island density over a wide range of coverages in simulations on a triangular lattice. These results ($z=1$ with a logarithmic correction and $\nu \simeq \frac{1}{2}$) are in agreement with the generalized rate-equation predictions [Eq. (20)] for the case $p=\frac{1}{2}$. As noted in Sec. III, for fractal islands with $d_f \simeq 1.7$ one has $p=1/d_f=0.58$, which implies $\nu=0.58$, $\gamma=0.79$, and $q=0.16$. For the highest value of R ($R=10^9$) a fit to the late part of this regime away from the peak of N_1 ($1.5\times10^{-3}<\theta<0.02$) gives $\nu \simeq 0.58$. Thus we find $\nu \simeq 0.5$–0.6.

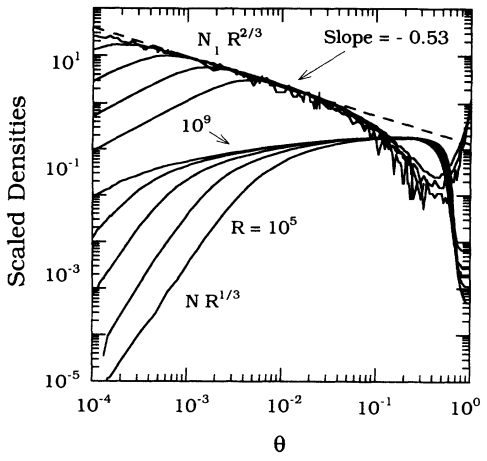

FIG. 4. Log-log scaling plot of $R^{\gamma}N_1$ and $R^{\chi}N$ as function of θ for $10^{-4}<\theta<1$ with $\gamma=\frac{2}{3}$ and $\chi=\frac{1}{3}$ and $R=10^5$–10^9. The dashed line is a power-law fit to the decay of the monomer density in the intermediate-coverage regime.

We have also studied the R dependence of the coefficient $A(R)$ in the intermediate coverage regime and obtain $A(R) \sim R^{-\chi}$ with $\chi=0.41$, somewhat below the predicted value [see Eq. (20)] of $\chi=\frac{1}{2}$ for $p=\frac{1}{2}$. In the limit $R \to \infty$ this scaling behavior predicts that the coefficient of logarithmic behavior goes to zero, so that asymptotically the island density becomes essentially independent of coverage in this regime. Thus the rate-equation analysis with $p \simeq \frac{1}{2}$ appears to account for the dynamical behavior of N_1 and N as well as approximately for the R dependence of N observed in the intermediate regime. However the R dependence of the monomer density N_1 is in closer agreement with the point-island prediction $\gamma=\frac{2}{3}$ than with the generalized rate-equation analysis (Sec. III) which predicts $\gamma=0.75$–0.79 for $p=0.5$–0.58.

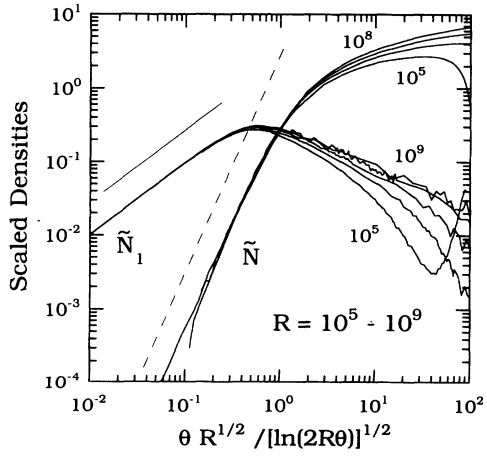

FIG. 3. Scaling plot showing the scaled densities $\tilde{N}_1=N_1R^{1/2}/[\ln(2R\theta)]^{1/2}$ and $\tilde{N}=NR^{1/2}$ vs $\theta R^{1/2}/[\ln(2R\theta)]^{1/2}$ in the early-time regime for $R=10^5$–10^8. The solid and dashed lines have slopes 1 and 3, respectively.

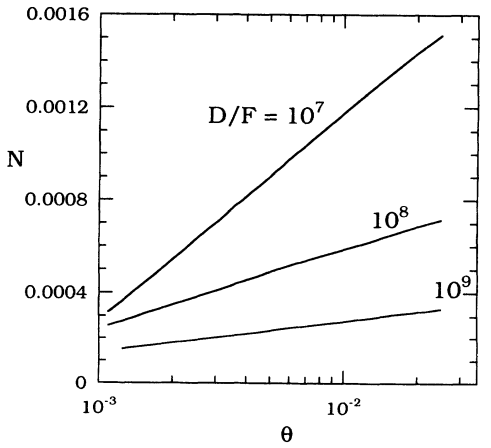

FIG. 5. Semilog plot of $N(\theta)$ in the intermediate time regime for $R=D/F=10^7$–10^9 showing logarithmic behavior $N \sim A(R)\ln(\theta)$.

C. Aggregation scaling regime $\theta_I < \theta < \theta_C$

1. Scaling of island density and monomer density

Beyond the intermediate regime ($\theta > \theta_I \simeq 0.02$, see Fig. 1), the monomer density decreases rapidly, and there is a rapid crossover from a regime in which $N_1 \sim \theta^{-\nu}$ with $\nu \simeq 0.5$ to a region of steeper slope with the maximum value of ν ranging from $\nu = 1.7$ for $R = 10^5$ to 2.5 for $R = 10^8$. However, this is not a true scaling region for the monomer density, since the slope is in fact increasing with R.[47] An analysis of the D/F dependence of the monomer density ($N_1 \sim R^{-\gamma}$) in this regime gives $\gamma = 0.75 \pm 0.05$, which is significantly larger than the point-island prediction $\gamma = \frac{2}{3}$ although close to the rate-equation result (21) for $p = 0.50-0.58$ which gives $\gamma = 0.75-0.79$.

In this regime ($\theta > 0.1$) one has $N_1 \ll \theta$, so that $S \simeq \theta/N$ and the ratio d/l of average cluster diameter d to average cluster distance l satisfies $d/l \sim \theta^{1/d_f}$. Consequently, the island diameter is of the order of the distance between islands, while the fraction of the surface occupied by islands is large enough that one must take into account the probability of deposition onto an island as well as onto the substrate. As a result every adatom deposited attaches to an existing island and no additional islands are created. This implies the existence of an extended aggregation regime for large D/F (up to coalescence) in which the island density $N \sim \theta^{1-z}$ remains approximately constant,[16,22,47] which implies $z = 1$. Beyond this regime, the islands begin to coalesce and the island density decreases rapidly with coverage.[49]

As can be seen from Fig. 4, the plateau region corresponding to the aggregation regime becomes wider and flatter with increasing R, in part due to the fact that $A(R)$ decreases with increasing R. For $R = 10^9$, the range of coverage over which the island density remains relatively constant is approximately $0.1 < \theta < 0.4$ (see Fig. 1). Interestingly, the value of the coverage at which the island density reaches its maximum value ($\theta_{\max} \simeq 0.172 \pm 0.003$) is essentially independent of R for $R \geq 10^5$.

From Fig. 4 one can also see that for large R ($R \geq 10^5$) the height of the plateau scales approximately as $N \sim R^{-\chi}$ with $\chi \simeq \frac{1}{3}$.[33,48] A power-law fit to the peak of the island density for $R = 10^5-10^9$ gives $N \simeq 0.43 R^{-0.34}$, while for smaller R the island density decreases more slowly. Thus the scaling of the island density as a function of R in the aggregation regime is in agreement with the prediction of the point-island rate equations, even though the dynamical behavior ($N \cong$ const) is not. These results imply that the average island size S scales as $S \sim R^{\chi}\theta^{z} \sim R^{1/3}\theta$ in the aggregation regime as shown in Fig. 6.

2. Island-size distribution scaling function

Figure 7(a) shows the island-size distribution $N_s(\theta)$ for $R = 10^9$ at four different values of θ in the aggregation regime. As θ increases, the position of the peak of the island-size distribution also increases while the peak

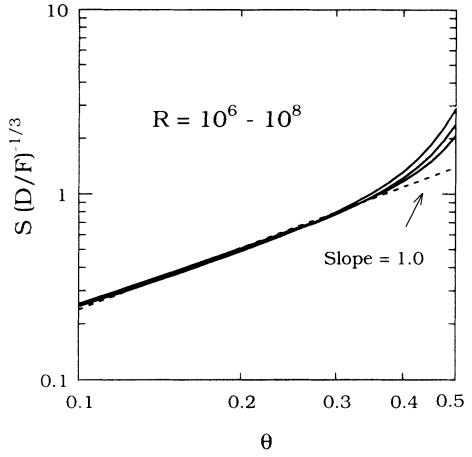

FIG. 6. Log-log plot of scaled average island size $S(D/F)^{-1/3}$ vs coverage θ in the aggregation regime for $D/F = 10^6-10^8$.

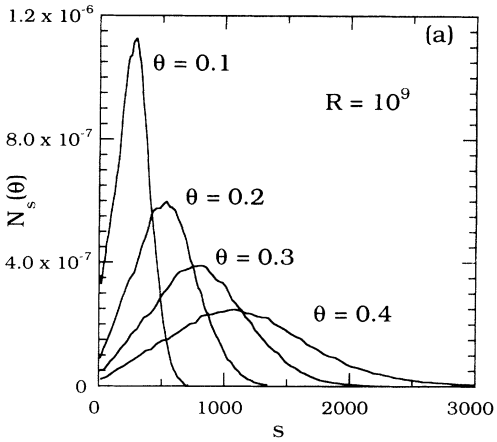

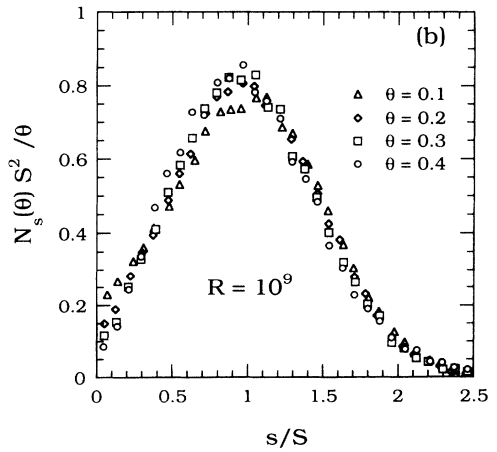

FIG. 7. (a) Unscaled island size distribution $N_s(\theta)$ in the aggregation regime for $R = 10^9$ and $\theta = 0.1-0.4$. (b) Scaled island size distribution $f(u)$ (scaled with average cluster size S) for $R = 10^9$ and $\theta = 0.1-0.4$.

height decreases. Since the island density is constant in this regime, one expects the island-size distribution function to satisfy scaling of the form of Eq. (3), with the island-size distribution $N_s(\theta)$ scaling with the average island size $S(\theta)$. Figure 7(b) shows plots of the island-size distribution scaling function $f(s/S)=S^2N_s(\theta)/\theta$ in the aggregation regime using the general scaling form (3) for $R=10^9$ and $\theta=0.1-0.4$. Similar plots for smaller values of R give essentially the same scaling function, but over a smaller range of θ since the coalescence regime sets in at lower coverage for smaller R. For $R=10^9$ and $\theta=0.5$ (not shown), scaling begins to break down due to island coalescence, and the scaled distribution begins to deviate from this form.

We note that the scaled island-size distribution $f(u)$ in our model in the aggregation regime is significantly different from the point-island rate equation solution at late time, which in our notation may be written[34]

$$f(u)=\begin{cases}\dfrac{1}{3}\left[1-\dfrac{2u}{3}\right]^{-1/2} & 0\le u\le\frac{3}{2}\\ 0 & u>\dfrac{3}{2}\ .\end{cases} \tag{22}$$

In particular, as shown in Fig. 7(b) the peak of the scaling function is finite and located at $u=1$ rather than $u=\frac{3}{2}$. Beyond the peak $f(u)$ remains finite rather than dropping to zero as predicted by the point-island result (22). Furthermore, the slope at $u=0$ is much larger (close to 1) than for the point-island model, while $f(0)$ is significantly smaller and appears to go to zero for large R. From the data for $R=10^7-10^9$ there appears to be a power-law scaling region [$f(u)\sim u^{\omega}$ with $\omega\simeq 0.8-0.9$] below the peak whose lower limit decreases as the coverage increases in the aggregation regime. However, it is difficult to calculate accurately the exponent ω since it appears to increase slightly as R increases. Log-log plots of the data in Fig. 7(b) as well as for $R=10^7-10^8$ (not shown) indicate that beyond the peak there is a rapid essentially exponential dropoff in the scaling function.

Since in this regime, one has $S\sim R^{1/3}\theta$, one may reexpress the island-size distribution using the scaling form (6) with $\chi=\frac{1}{3}$ and $z=\tau=1$. Scaling plots of this form for $\theta=0.1-0.3$ and $R=10^7-10^9$ are shown in Fig. 8. As one can see, there is reasonable scaling in this regime for the whole range of coverage up to $\theta=0.3$, and for all values of R. However, for large enough coverage, the distribution changes radically due to coalescence. A dramatic example of this behavior for $R=10^7$ and $\theta=0.5$ is shown, where the extended (approximately power-law) tail is due to coalescence.

3. *Scaling of structure factor and pair-correlation function*

In order to obtain more information about the geometry and spatial correlations in the aggregation regime, we have also studied the scaling of the adlayer structure factor $S(\mathbf{k})$ and pair-correlation function $G(\mathbf{r})$ as functions of R and θ in both the aggregation and coalescence regimes. While the island-size distribution is relatively sensitive to coalescence, the structure factor $S(\mathbf{k})$ is not, although it is more sensitive to the island geometry.[50] Taking the density $n(\mathbf{r})$ to be 1 at a site $\mathbf{r}$ at which there is an adlayer atom, and 0 otherwise, we calculated the circularly averaged adlayer density-density pair-correlation function $G(r)=\langle\tilde{n}(\mathbf{0})\tilde{n}(\mathbf{r})\rangle_c$, where $\tilde{n}(\mathbf{r})=n(\mathbf{r})-\theta$ and $G(0)=\theta-\theta^2$. The brackets denote a circular average as well as an average over runs. We also calculated the (normalized) circularly averaged structure factor $S(k)$, where

$$S(k)=\left\langle\frac{1}{L^2}\left|\sum_{\mathbf{r}}\tilde{n}(\mathbf{r})e^{i\mathbf{k}\cdot\mathbf{r}}\right|^2\right\rangle_c =\left\langle\sum_{\mathbf{r}}\langle\tilde{n}(\mathbf{0})\tilde{n}(\mathbf{r})\rangle e^{-i\mathbf{k}\cdot\mathbf{r}}\right\rangle_c . \tag{23}$$

We note that the adlayer structure factor $S(\mathbf{k})$ is essentially equivalent to the "diffuse" diffracted intensity profile $I(\mathbf{k})$ for momentum transfer with lateral component $\mathbf{k}$ and vertical component k_z. Assuming the amplitude for scattering by the adlayer is 1, and for the substrate is given by A, one has

$$I(\mathbf{k},k_z)\sim(2\pi^2)|\theta+(1-\theta)Ae^{ik_za}|^2\delta(\mathbf{k}) +|1-Ae^{ik_za}|^2S(\mathbf{k})\ . \tag{24}$$

Figure 9(a) shows typical plots of the circularly averaged structure factor in the aggregation regime for $D/F=10^5-10^9$ at $\theta=0.2$. The position (k_m) of the peak in $S(k)$ corresponds to the typical island distance l ($k_m\sim 1/l\sim N^{1/2}$) and therefore decreases with increasing R, while the height of the peak increases with increasing R. In particular, since one has $N\sim R^{-1/3}$ in the aggregation regime, one expects $k_m\sim R^{-1/6}$. Figure 9(b) verifies this dependence for $\theta=0.2$. For higher values of θ in the aggregation regime, k_m is essentially unchanged since the island density N remains constant, while for $\theta=0.1$, at the very beginning of the aggregation regime, k_m is slightly smaller for a given R (due to the decreased island density) and we find $k_m\sim R^{-0.18}$.

One interesting question is the scaling of the circularly

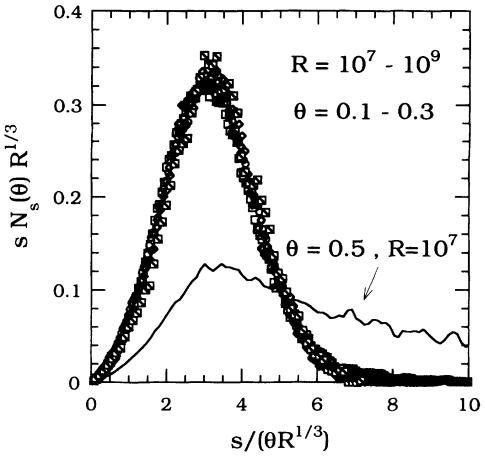

FIG. 8. Scaling plot for the island size distribution using Eq. (6) with $\tau=z=1$ and $\chi=\frac{1}{3}$ for $R=10^7-10^9$.

averaged structure factor $S(k;R,\theta)$ for fixed coverage θ in the aggregation regime as a function of D/F. For compact islands, one expects that for fixed θ the average island diameter d scales as $d \sim l \sim S^{1/2} \sim (\theta/N)^{1/2} \sim R^{1/6}$, where l is the average island spacing. Thus for fixed coverage there is only one length scale $d \sim l \sim k_m^{-1}$, and (assuming no change in island shape as a function of size) one expects the (circularly averaged) pair-correlation function to scale as

$$G(r;R,\theta) = f_G(rk_m;\theta) , \tag{25a}$$

which for $S(k)$ implies

$$S(k;R,\theta) = k_m^{-2} f_S(k/k_m;\theta) , \tag{25b}$$

where the R dependence is given by $k_m \sim R^{-1/6}$.

However, in the beginning of the aggregation regime ($\theta \simeq 0.1$) and for the range of R ($R = 10^5 - 10^9$) studied here, the islands are fractal. (For larger θ one expects that the islands will become compact due to the filling in of the clusters as adatoms land on top of and in between the arms.) In Fig. 10 the island size s is shown to scale as $s \sim R_G^{d_f}$, where R_G is the radius of gyration of each island

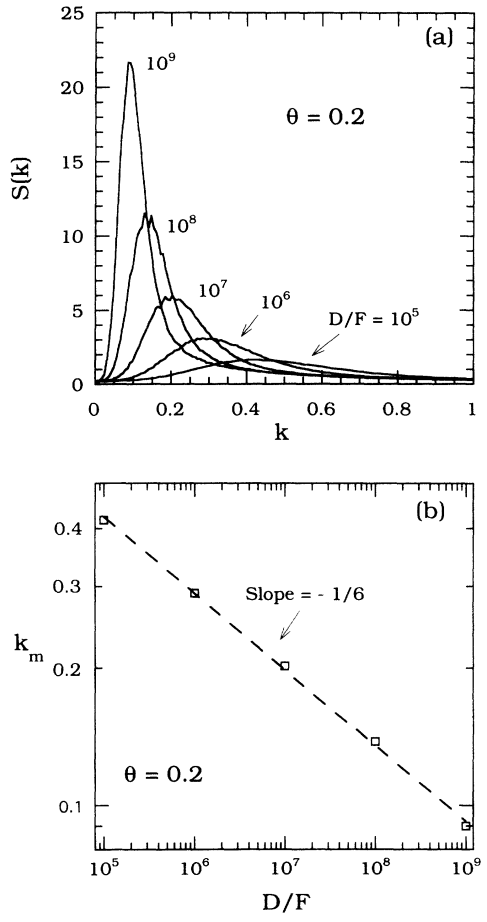

FIG. 9. (a) Circularly averaged structure factor $S(k)$ at coverage $\theta = 0.2$ and $D/F = 10^5 - 10^9$. (b) Log-log plot of peak position k_m as a function of D/F in the aggregation regime. Straight-line fit has slope $-\frac{1}{6}$.

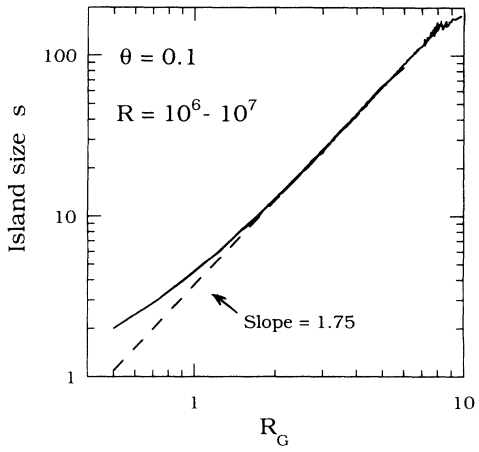

FIG. 10. Log-log plot of island size vs radius of gyration R_G for $\theta = 0.1$ and $D/F = 10^6 - 10^7$. Dashed-line fit has slope 1.75.

and $d_f \simeq 1.75$ for $\theta = 0.1$. This is consistent with the fractal dimension of diffusion-limited aggregation (DLA).[51] Thus there are essentially two length scales which vary differently as a function of R: the average island distance $l \sim N^{-1/2} \sim R^{1/6}$ and the average cluster diameter $d \sim S^{1/d_f} \sim (\theta/N)^{1/d_f} \sim l^{2/d_f}$. This implies that no single scaling form will exactly scale the structure factor for all k as a function of R, even for fixed coverage. However, we can write an approximate scaling form similar to Eq. (25) using the following argument.

We assume for simplicity that the islands consist of a set of identical clusters (which may or may not be randomly distributed). In this case (taking the density to be 1 at an occupied site and 0 at an unoccupied site) one may rewrite the structure factor $S(\mathbf{k})$ for $\mathbf{k} \neq \mathbf{0}$ as the product of a form factor $S_1(\mathbf{k})$ for each cluster, and the structure factor $S_2(\mathbf{k})$ for a distribution of point particles at the center of each cluster. For fixed coverage θ but varying R (assuming the same distribution of island centers but simply rescaled for different R), for the circularly averaged structure factor one may write $S_2(k,R) = k_m^2 \phi_2(k/k_m)$, where k_m^2 is proportional to the density of islands. For fixed coverage, the average cluster size scales as $S \sim \theta N^{-1} \sim k_m^{-2}$, and the average cluster diameter as $d \sim k_m^{-2/d_f}$, so that one may write $S_1(k;R) \sim k_m^{-4} \phi_1(k/k_m^{2/d_f})$, where ϕ_1 is a crossover function and the factor of k_m^{-4} comes from the square of the average cluster size. Combining the two expressions, one has

$$S(k;R,\theta) = f(\theta) k_m^{-2} \phi_1(k/k_m^{2/d_f}) \phi_2(k/k_m) , \tag{26}$$

where $\phi_1(u) \simeq u^{-d_f}$ for $1 \leq u < d/a$ (where a is a short-distance crossover length scale) and $\phi_1(u) = 1$ for $u \ll 1$. A factor of $f(\theta)$ has been included to approximately account for the coverage dependence. The function $\phi_2(u)$ is expected to be sharply peaked at $u = 1$, corresponding to the average island distance. Of course, given the situation in which the islands are relatively randomly distributed and have a range of different sizes, this expression is only approximate. In particular, the dispersion in island sizes and distances may allow an overlap between

the power-law scaling region of $\phi_1(u)$ and the peak in $\phi_2(u)$. For $d_f=2$, we recover Eq. (25b).

We now consider the scaling of the peak of $S(k;R,\theta)$ as a function of R for fixed θ. Assuming that $\phi_1(u)\sim u^{-d_f}$ for $u\simeq 1\,(k\simeq k_m)$, Eq. (26) becomes $S(k_m;R,\theta)=f(\theta)k_m^{-d_f}\phi_2(k/k_m)$. Since the peak dominates the structure factor, one may then write the approximate scaling form

$$S(k;R,\theta)\simeq k_m^{-d_f} f_S(k/k_m) f(\theta)\ , \tag{27a}$$

where again the R dependence is given by $k_m\sim R^{-1/6}$. Taking the Fourier transform, this implies that the pair-correlation function satisfies the approximate scaling form:[52]

$$G(r;R,\theta)\simeq k_m^{2-d_f} f_G(rk_m) f(\theta)\ . \tag{27b}$$

We note that since $G(0;R,\theta)=\theta-\theta^2$, this implies that for fixed coverage $f_G(0)\sim k_m^{d_f-2}\sim R^{(2-d_f)/6}$. Thus the scaling function $f_G(u)$ has the unusual property that it scales (approximately) everywhere except at $u=0$. This reflects the fact that the scaling form (27a) does not work well for large k (i.e., for $k\gg k_m$), where the structure factor is very small.

Figure 11(a) shows a scaling plot for the structure factor $S(k)$ for $\theta=0.1$ and $R=10^6$–10^9 using (27a) with $d_f=1.7$. Corresponding scaling plots for $G(r)$ are shown in Fig. 11(b). As one can see, the scaling is very good, while similar plots using $d_f=2$ (not shown) give very poor scaling. Surprisingly, we also find excellent scaling (Fig. 12) using Eq. (27) with $d_f=1.7$ for higher coverages ($\theta=0.2$–0.5), even though the clusters are essentially compact over this coverage range (see Fig. 13 and Table I). This appears to be due to the fact that although the core of the clusters has become compact, they continue to generate dendritic DLA-like branches as shown in Fig. 2. The existence of this anomalous scaling form for the structure factor should be useful as an experimental signature for the identification of dendritic islands.

In addition to scaling the (circularly averaged) structure factor $S(k;R,\theta)$ and pair-correlation function $G(r;R,\theta)$ for fixed coverage as functions of R, we can also approximate the coverage dependence given by the scaling function $f(\theta)$. We do this by noting that $G(\mathbf{0})=\theta-\theta^2=\int S(\mathbf{k})d^2\mathbf{k}$ and $S(\mathbf{0})=0=\int G(\mathbf{r})d^2\mathbf{r}$, while $S(\infty)=G(\infty)=0$. Thus the normalized circularly averaged pair-correlation function $\tilde{G}(r;R,\theta)=(\theta-\theta^2)^{-1}G(r;R,\theta)$ satisfies the three conditions $\tilde{G}(0;R,\theta)=1$, $\int\tilde{G}(r;R,\theta)dr=0$, and $\tilde{G}(\infty;R,\theta)=0$, while the normalized circularly averaged structure factor $\tilde{S}(k;R,\theta)=(\theta-\theta^2)^{-1}S(k;R,\theta)$ satisfies the three conditions $\tilde{S}(0;R,\theta)=0$, $\int\tilde{S}(k;R,\theta)dk=1$, and $\tilde{S}(\infty;R,\theta)=0$. Given these three constraints on $\tilde{G}$ and $\tilde{S}$, and the fact that k_m is essentially independent of θ in the aggregation regime, one expects that, for fixed R (fixed k_m), $\tilde{G}$ and $\tilde{S}$ will be almost independent of θ. Thus we may write $f(\theta)\simeq(\theta-\theta^2)$ in Eq. (27). A scaling plot of $S(k)$ using this form with $R=10^8$ and $\theta=0.1$–0.5 is shown in Fig. 14. The peak value scales within 10–20% for the whole range of θ. Similar plots have been made for the circularly averaged correlation function $G(r)$. Thus we are able to scale approximately all our data for $S(k)$ and $G(r)$ in the aggregation regime both as a function of R (for $R=10^5$–10^9) and as a function of coverage (for $\theta=0.1$–0.5) using the scaling form (27) with

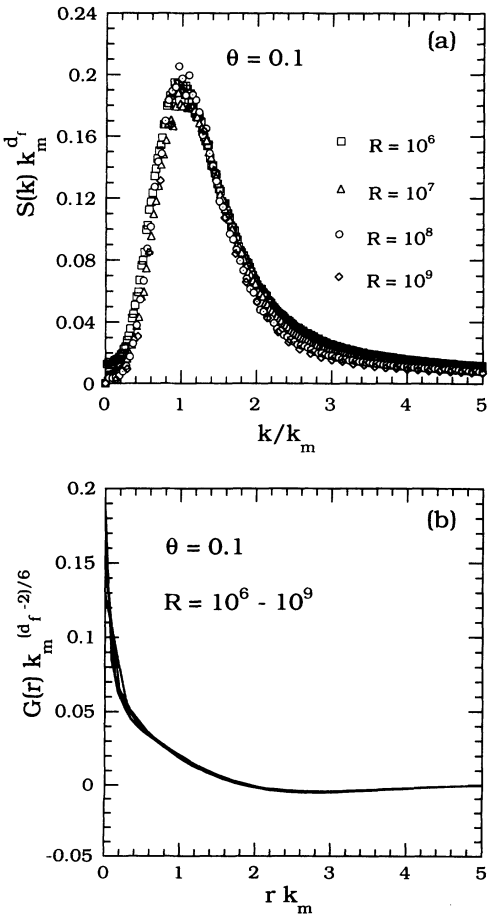

FIG. 11. (a) Structure factor scaling plot of form of Eq. (27) at $\theta=0.1$ showing scaling for $D/F=10^6$–10^9 with $d_f=1.7$. (b) Same as (a) but for correlation function $G(r)$.

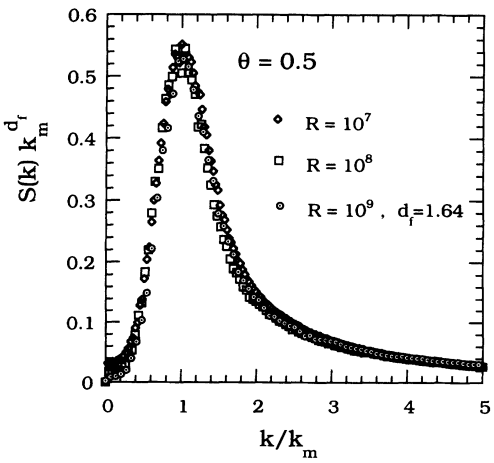

FIG. 12. Scaling plot for structure factor $S(k)$ at $\theta=0.5$ showing scaling for $R=10^7$–10^9 with $d_f\simeq 1.7$.

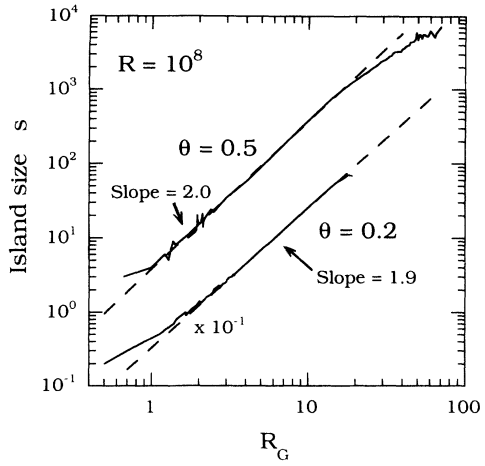

FIG. 13. Log-log plots of island size vs radius of gyration R_G for $\theta=0.2$ and $\theta=0.5$. The bending over of the curve at large R_G for $\theta=0.5$ is due to cluster coalescence.

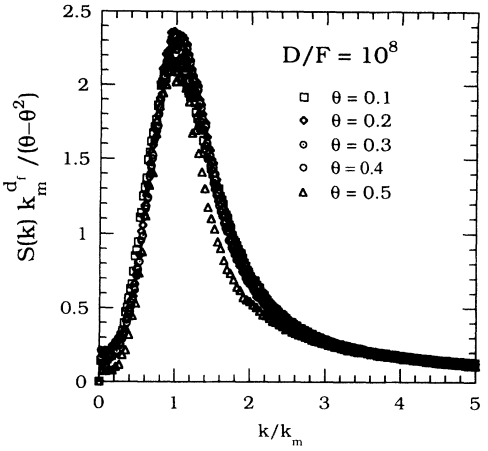

FIG. 14. Combined scaling plots for $S(k)/(\theta-\theta^2)$ for different θ and $D/F=10^8$.

$f(\theta)=\theta-\theta^2$ and $d_f\simeq 1.7$.

We can explicitly derive the form of $f(\theta)$ in the limit of low coverage by modifying the arguments used in deriving Eq. (26) to include the coverage dependence. Specifically, we write $d\sim(\theta/N)^{1/d_f}\sim(\theta/k_m^2)^{1/d_f}$, where $S=\theta/N$ is the mass of the average cluster. Then one has $S_1(k;R,\theta)\sim\theta^2k_m^{-4}\phi_1(k\theta^{1/d_f}/k_m^{2/d_f})$, where the factor of $\theta^2k_m^{-4}$ comes from the square of the mass of the average island. Equation (26) then becomes $S(k;R,\theta)=\theta^2k_m^{-2}\phi_1(k\theta^{1/d_f}/k_m^{2/d_f})\phi_2(k/k_m)$. Considering the behavior near the peak as before [where $\phi_1(u)\sim u^{-d_f}$], one then obtains $S(k;R,\theta)\simeq\theta k_m^{-d_f}f_S(k/k_m)$ for $k\simeq k_m$. This implies that in the low-coverage limit $\theta\to 0$ (which is the limit to which the pure fractal case applies) $f(\theta)\sim\theta$, in agreement with the form used in Fig. 14.

We now consider the scaling of $S(k;R,\theta)$ for large k ($k\gg k_m$). For $k_m\ll k<d/a$, one expects that the dominant contribution to the k dependence of $S(k)$ will come from the form factor of individual clusters, since this region of k corresponds to length scales much smaller than the average intercluster separation. In particular, for $k_m\ll k<d/a$ we again take $S_1(k)=k_m^{-4}\phi_1(k/k_m^{2/d_f})\sim k_m^{-2}k^{-d_f}$, while we assume that the k_m dependence of $S_2(k)$ is given by $S_2(k)\sim k_m^2\phi_2(k/k_m)$, where $\phi_2(k/k_m)$ is approximately constant. This corresponds to assuming that the interisland contributions to $S(k)$ are essentially constant (independent of k and k_m) for large k. Thus one obtains

$$S(k;R,\theta)\sim(\theta-\theta^2)k^{-d_f}\ ,\quad k_m\ll k<d/a\ . \tag{28}$$

This implies that $S(k;R,\theta)$ scales differently as a function of R for large k than for k near k_m. Figure 15 shows log-log plots of $S(k)$ for $\theta=0.1$ and $R=10^6-10^9$ which demonstrate this scaling form for large k. The slight bend in $S(k)$ at the largest values of k corresponds to the crossover region at the beginning of our mass versus R_G plots, while the region of power-law scaling in k corresponds to the region in which one sees linear behavior in log-log plots of mass versus R_G. For $\theta=0.1$, the absolute value of the slope in the scaling region is 1.3 which is somewhat less than the measured $d_f\simeq 1.7$. However, this is not totally surprising, since it has been shown[53] that for small fractal systems with short crossover

TABLE I. Island fractal dimension d_f determined from fits to the linear region in log-log plots of island size s vs radius of gyration R_G. Note that d_f increases strongly as θ increases, while there is a much weaker dependence on R.

	Coverage θ				
R	0.1	0.2	0.3	0.4	0.5
10^6	1.72	1.86	1.88	1.99	2.04
10^7	1.78	1.89	1.93	1.99	2.08
10^8	1.81	1.91	1.97	2.00	2.07

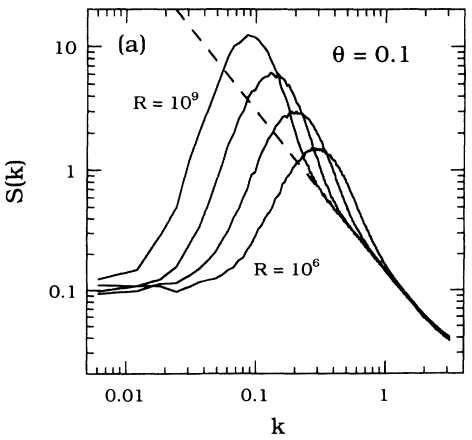

FIG. 15. Log-log plot of $S(k)$ at $\theta=0.1$ and $D/F=10^6-10^9$ showing scaling behavior for large k. Slope of dashed line is -1.32.

lengths, one often obtains effective exponents in $S(k)$ which are somewhat smaller than the actual fractal dimension. Similar plots have been made for higher values of the coverage, and power-law behavior of $S(k)$ was also observed for large k. For example, for $\theta=0.5$ and $D/F=10^8$ the absolute value of the slope for large k (1.66) is significantly larger than for $\theta=0.1$ due to the increased compactness of the clusters.

D. Coalescence and percolation regime ($\theta > \theta_C$)

Beyond the aggregation regime the islands begin to coalesce and eventually percolate, so that the island density rapidly decreases while the monomer density increases due to the formation of a second layer. As already noted, as R increases in the scaling regime ($R \geq 10^5$), the plateau region of the island density flattens and widens so that θ_C increases with increasing R. This suggests that the percolation coverage θ_p should increase with increasing R. However, for small R ($R \leq 10^4$) the coalescence portion of the scaled island density curves (not shown) shifts to lower coverages as R increases, implying that θ_p should decrease with increasing R for $R < 10^4$. Thus the percolation coverage θ_p should exhibit nonmonotonic behavior as a function of R, with a minimum near $R=10^4$.

In order to study this behavior more carefully, we have studied the critical total coverage at percolation $\theta_p(R;L)$ for different system sizes L as a function of R. We also kept track of the first-layer coverage at percolation $\theta_{1p}(R;L)$. The clusters were identified using a simple recursive algorithm, while the percolation condition was defined as corresponding to a cluster which spans the system size L in the horizontal direction. Simulations were conducted for $L=300$, 400, and 500 and $L=1000$ and $R=10^1-10^9$. From the data for $\theta_p(R;L)$ for each value of R, the infinite system percolation coverage was estimated using the finite-size-scaling form, $\theta_p(\infty)-\theta_p(L)=CL^{-1/\nu}$, where $\nu=\frac{4}{3}$ for ordinary percolation. Percolation and finite size effects have also been studied in a model that includes cluster diffusion.[54] Figure 16 shows a typical finite-size-scaling plot for $\theta_p(R;L)$ with $R=10^6$, while Fig. 17 shows typical pictures of the percolating cluster for various values of $R=D/F$. We note that as R increases, the typical "blob" size at percolation increases due to the decreasing density of islands.

Our results for θ_p and θ_{1p} as a function of $R=D/F$ are shown in Fig. 18. The percolation coverage θ_p exhibits strong nonmonotonic behavior as a function of R, with a minimum near $R=10^4$, just below the range of R for which scaling of the island density $N \sim R^{-\chi}$ with $\chi=\frac{1}{3}$ sets in. The estimated first-layer coverage at percolation θ_{1p} is also shown, indicating that there is significant second-layer growth before percolation for $R < 10^4$. This is shown more clearly by the pictures in Fig. 19. The existence of significant second-layer growth before percolation is due to the fact that for small D/F the diffusion length $l_D \sim \sqrt{D/F}$ is of the order of the typical cluster diameter d at percolation. However, for

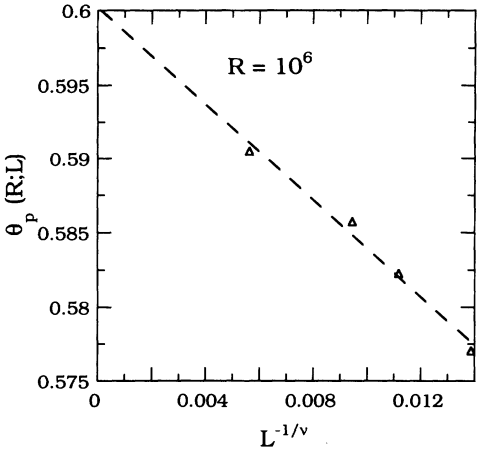

FIG. 16. Finite-size scaling plot of $\theta_p(R;L)$ vs $L^{-1/\nu}$ with $\nu=\frac{4}{3}$, $R=10^6$, and $L=300$, 400, 500, and 1000.

$R > 10^4$ one has $l_D \gg d$ and therefore there is no second-layer growth and $\theta_{1p} \simeq \theta_p$. Thus the decrease in θ_p with increasing R for $R < 10^4$ is mainly due to the decrease in second-layer growth.

Interestingly, the first-layer percolation coverage $\theta_{1p}(R)$ also exhibits a minimum for $R \simeq 10^2$, somewhat below the minimum for θ_p. Similar nonmonotonic behavior has been previously observed in models of correlated percolation[55,56] as a function of the ratio of the probability of nucleation to the sticking probability. This behavior can be explained in terms of a change of morphology of the clusters. For small R the clusters in the first layer are like those for ordinary percolation, and as $R \to 0$, $\theta_{1p} \to p_c^{\text{site}} \simeq 0.593$.[54] As the diffusion increases, the clusters become stringy (see Fig. 19), and this enhances percolation and reduces θ_{1p}, while for large enough R an increase in R leads to an increase in the smoothness of the clusters and an increase in θ_{1p} as discussed below.

We can also use the value of $\theta_{1p}(R=0)$ to calculate $\theta_p(R=0)$ exactly. Taking into account the probability of deposition at a site in which the first layer is already occupied, one has $d\theta_1=(1-\theta_1)d\theta$, where $(1-\theta_1)$ is the probability of depositing on top of an empty site. Integrating, one obtains $\theta_p(0)=\ln(1/[1-\theta_{1p}(0)])$, and substituting the value of $\theta_{1p}(R=0)$ yields $\theta_p(R=0) \simeq 0.898$.

Perhaps the most interesting result is the increase of θ_p with increasing R for $R > 10^4$. A simple explanation of this increase is as follows.[56] As R increases, the clusters (which are relatively compact near percolation) become larger. Assuming that the fluctuations (roughness) at the surface of a cluster increase less rapidly than the cluster size as a function of R, then the relative roughness decreases with increasing R. This is consistent with the increase in compactness as R increases, which is shown in Table I. As their relative roughness decreases, nearby clusters are less likely to touch and consequently the percolation coverage increases. Thus, while the decrease in $\theta_p(R)$ for $R < 10^4$ is due to the decrease of second-layer growth, the increase of $\theta_p(R)$ with increasing R for

$R > 10^5$ is due to the increasing smoothness and compactness of the clusters. A nonmonotonic dependence of θ_p on D/F has also been observed in recent simulations of square-island growth.[50]

One interesting question is the limit of $\theta_p(R)$ as $R \to \infty$. Assuming no correlation between the cluster positions, θ_p should tend to the continuum percolation limit $\theta_p \simeq 0.67$[57] since in this limit the clusters correspond to large smooth circular disks. We note that for $R = 10^9$, we already have $\theta_p \simeq 0.66$, close to the continuum percolation limit. Thus it is quite likely that $\theta_p(\infty)$ is larger than the continuum percolation limit. This is reasonable, given the existence of correlations in the cluster positions due to the decreased probability that a cluster will be formed near an existing cluster. This is also consistent with recent experimental work[58] on thermal evaporation of metals on warm substrates, in which an unusually large first-layer percolation coverage ($\theta_{1p} \simeq 0.8$) was observed.

VI. CONCLUSION

Understanding the evolution of the submonolayer in epitaxial growth is an important first step in the study of the mechanisms of thin-film growth. Recently, the island distribution and morphology in submonolayer epitaxial growth have been observed in a number of experiments[18–20,23,25–28] on a variety of different systems and under a range of different conditions, and in a number of these experiments[23,25–28] dendritic islands were observed.

In this paper we have investigated the evolution, growth, and scaling of the island size, density, and distribution as a function of the coverage θ and D/F in a mod-

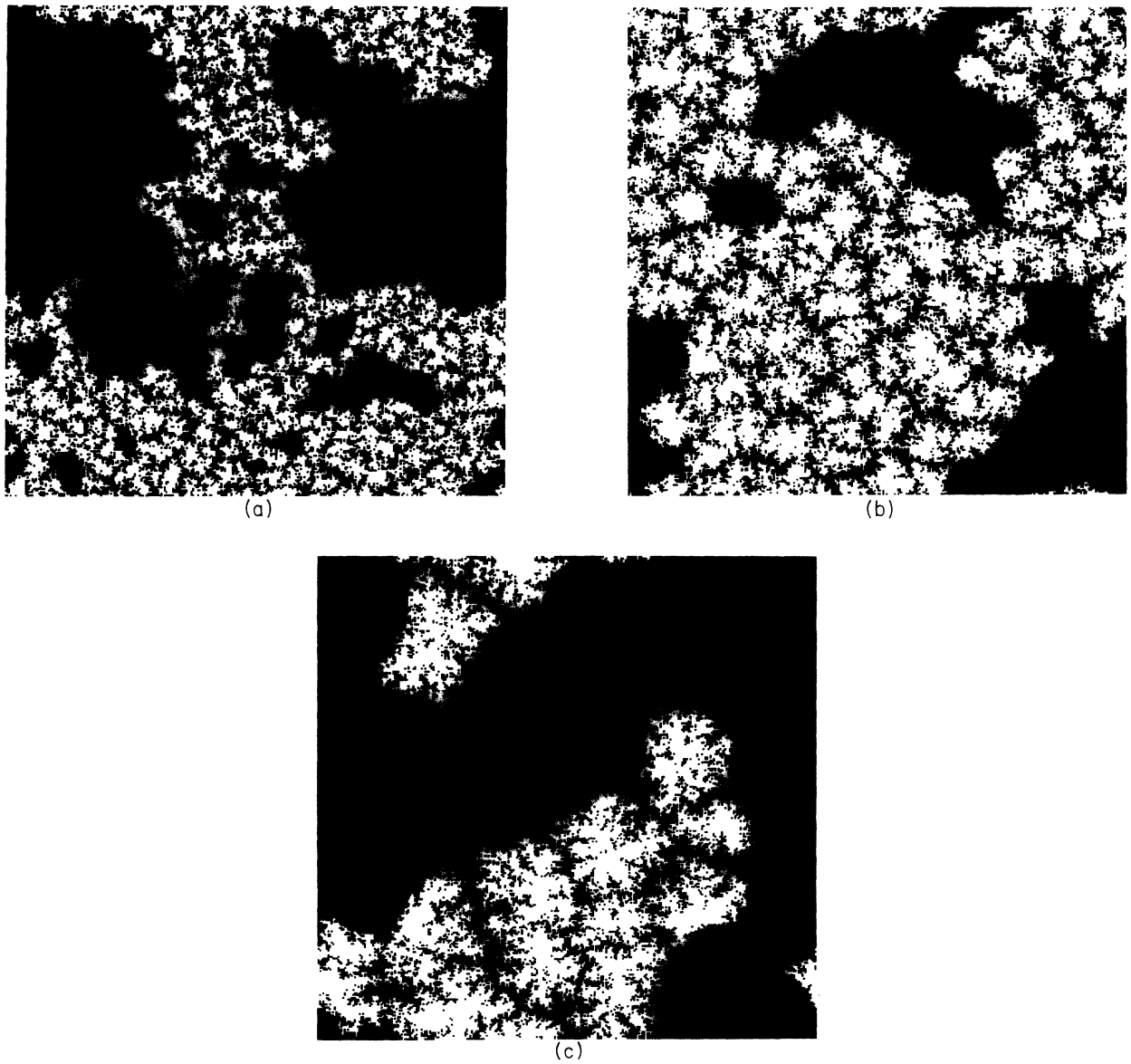

FIG. 17. Pictures of spanning cluster at percolation (white) for system size $L = 300$ and large R. (a) $R = 10^5$. (b) $R = 10^7$. (c) $R = 10^9$. Gray areas correspond to islands which are not part of the spanning cluster, while the black correspond to empty regions.

el of molecular-beam epitaxy appropriate for the case of dendritic island growth. Our Monte Carlo results span the range from very low coverage through the coalescence and percolation regimes. In addition, we have presented a scaling theory and rate-equation analysis, with appropriate modifications for the case of fractal islands. While some of our results (such as the anomalous scaling of the structure factor as a function of $R=D/F$) are only appropriate for the case of dendritic island growth, we expect others (such as the existence of four distinct scaling regimes as a function of coverage, or the coverage dependence of the structure factor) to apply to either the pure compact or the fractal case. We now summarize our results.

In the early-time low-coverage nucleation regime, we found good agreement with the predictions of the point-island model.[33,34] However, beyond the nucleation regime we found substantial deviations from the dynamical behavior predicted by the point-island model and rate equations. In particular, in the intermediate-coverage regime we found $N_1 \sim \theta^{-\nu}$ with $\nu \simeq 0.5$ and $N \sim \theta^{1-z} \sim \ln(\theta)$ with $z=1$, in contrast to the point-island predictions $\nu=\frac{1}{3}$ and $z=\frac{2}{3}$. As already noted, these results are in rough agreement with the predictions of the generalized rate equations [see Eq. (20)] modified to take into account the finite size of islands by including a power-law dependence of the aggregation rate on the island size with $p=\frac{1}{2}$. However, our results for the scaling of the monomer density as a function of R in this regime ($N_1 \sim R^{-\gamma}$ with $\gamma \simeq \frac{2}{3}$) agree surprisingly well with the predictions of the point-island rate equations.

Beyond the intermediate-coverage regime we found, again in contrast to the predictions of the point-island model, an extended aggregation regime for which the island density remains constant ($z=1$) while the monomer density rapidly decreases. The existence of this regime is due to the finite extent of the islands. We note that such a regime has recently been observed by Li, Vidali, and Biham[22] in recent experiments on compact island growth for Pb/Cu(001). The range of this extended aggregation regime was found to increase as D/F is increased, spanning a range of $0.1<\theta<0.4$ for $D/F=10^9$. As already noted, this is consistent with our prediction of the decrease of the coefficient $A(R)$ in the expression $N \sim A(R)\ln(\theta)$ with increasing R in the intermediate-coverage region [see Eq. (20)].

Surprisingly, we found that although the dynamics in the aggregation regime is substantially different from that for the point-island model, the R dependence of the island density at fixed coverage ($N \sim R^{-\chi}$ with $\chi \simeq \frac{1}{3}$) is in good agreement with the point-island prediction. We also found excellent scaling of the island-size distribution using the generalized scaling form $N_s(\theta)=\theta S^{-2} f(s/S)$ as

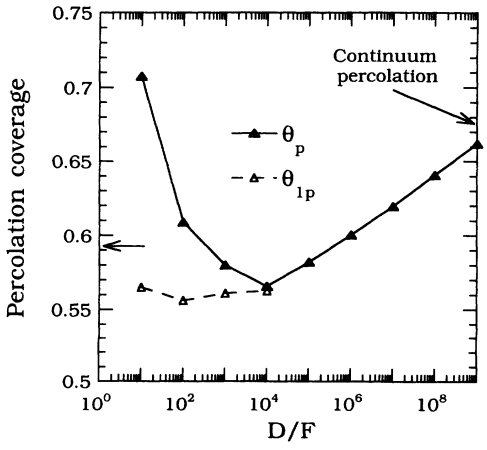

FIG. 18. Percolation coverage θ_p and first-layer coverage at percolation θ_{1p} vs D/F. Arrow at left of graph corresponds to ordinary site percolation ($D/F=0$).

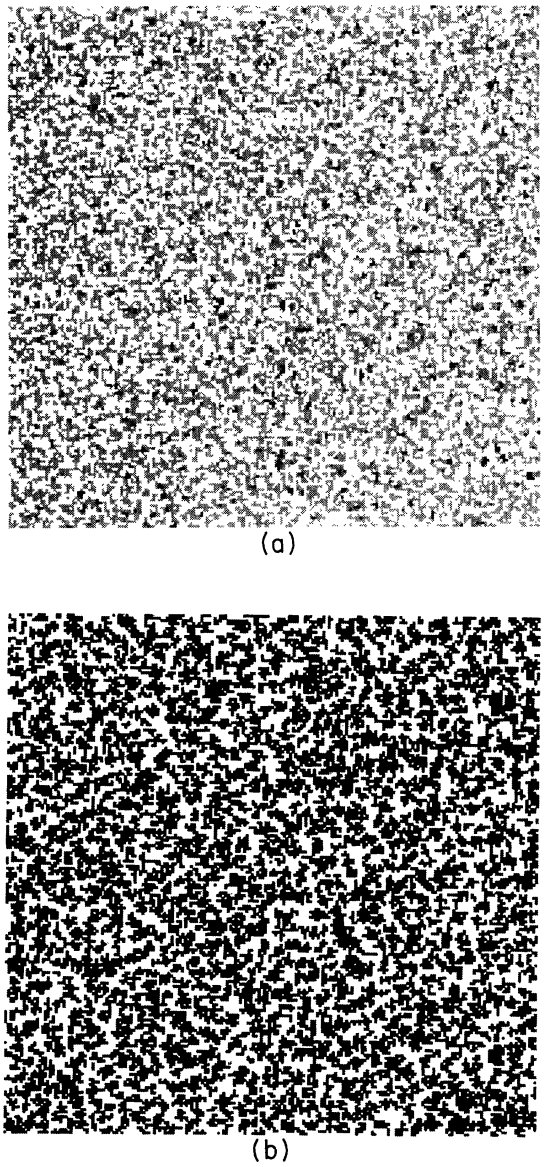

FIG. 19. (a) Gray-scale plot ($L=200$) of island morphology for $R=10^2$ and $\theta=0.5$ showing first-layer (light gray), second layer (dark gray), and some third-layer (black) growth. (b) Gray-scale plot ($L=200$) of island morphology for $R=10^3$ and $\theta=0.5$ showing first- (gray) and second-layer (black) growth.

well as using Eq. (6) with $z=\tau=1$ and $\chi=\frac{1}{3}$ in the aggregation regime for a wide range of R and θ. As expected, the island-size distribution scaling function $f(u)$ ($u=s/S$) is significantly different from that obtained from the point-island rate equations. At higher coverage, however, the island-size distribution no longer scales, and develops a long (approximately power-law) tail due to coalescence.

Our results for the morphology of the islands and the fractal dimension d_f in the aggregation regime are in good agreement with the qualitative behavior observed in Au/Ru(0001). As expected, we found that the clusters become more compact with increasing coverage, while there is also a slight increase in d_f as R increases. For large R ($R=10^5-10^9$) we found that for $\theta=0.1$ the islands are fractal ($d_f\simeq 1.7$), while for $\theta=0.5$ they are compact ($d_f\simeq 2$).

We also investigated the scaling of the circularly averaged structure $S(k)$ and pair-correlation function $G(r)$ in and beyond the aggregation regime. We found that the scaling of the structure factor peak for $k\neq 0$ [and of $G(r)$ for $r\neq 0$] as a function of R satisfies an anomalous fractal scaling form with $d_f\simeq 1.7$, which we derived for fractal clusters using a simple scaling analysis. We found that this anomalous scaling form with $d_f\simeq 1.7$ also holds for the entire range of coverage in and even somewhat beyond the aggregation regime ($\theta=0.1-0.5$), even though for $\theta\geq 0.2$ the clusters have become significantly more compact. As already noted, this appears to be due to the fact that although the core of the clusters becomes compact, they continue to generate dendritic DLA-like branches. The existence of this anomalous scaling form for the structure factor should be useful as an experimental signature for the identification of dendritic islands. For large k, we found that the power-law tail of the structure factor satisfies a different scaling form [Eq. (28)], with an exponent somewhat below the cluster fractal dimension. We also found that we were able to approximately scale both $S(k;\theta)$ and $G(r;\theta)$ for different coverages, using the approximate normalization factor $f(\theta)=(\theta-\theta^2)$.

Finally, we studied the percolation coverage θ_p as a function of $R=D/F$. For small R ($R<10^4$) there is significant second-layer growth before percolation, and θ_p decreases with increasing R due to the decrease in second-layer growth with increasing R. However, for large R ($R\geq 10^5$) there is negligible second-layer growth before percolation, and the percolation coverage θ_p increases with increasing R due to the increasing compactness of the clusters. Thus our results for the percolation behavior as a function of R for large R have important implications for the understanding of multilayer growth.

ACKNOWLEDGMENTS

This work was supported by National Science Foundation Grant No. DMR-9214308, and by the Office of Naval Research.

*Present address.

[1]J. W. Matthews, *Epitaxial Growth* (Academic, New York, 1975).

[2]B. Lewis and J. C. Anderson, *Nucleation and Growth of Thin Films* (Academic, New York, 1978).

[3]J. Y. Tsao, *Materials Fundamentals of Molecular Beam Epitaxy* (World Scientific, Singapore, 1993).

[4]M. von Smoluchowski, Z. Phys. Chem. **17**, 557 (1916).

[5]M. von Smoluchowski, Z. Phys. Chem. **92**, 129 (1917).

[6]T. Vicsek and F. Family, Phys. Rev. Lett. **52**, 1669 (1984).

[7]W. W. Mullins, J. Appl. Phys. **59**, 1341 (1986).

[8]F. Family and P. Meakin, Phys. Rev. Lett. **61**, 428 (1988).

[9]P. Meakin, T. Vicsek, and F. Family, Phys. Rev. B **31**, 564 (1985).

[10]R. Botet and R. Jullien, J. Phys. A **17**, 2517 (1984).

[11]F. Family, P. Meakin, and T. Vicsek, J. Chem. Phys. **83**, 4144 (1985).

[12]P. Meakin, in *Phase Transitions and Critical Phenomena*, edited by C. Domb and J. Lebowitz (Academic, New York, 1988), Vol. 12.

[13]F. Family, P. Meakin, and J. M. Deutch, Phys. Rev. Lett. **57**, 727 (1986).

[14]F. Family and P. Meakin, Phys. Rev. A **40**, 3836 (1989).

[15]M. Zinke-Allmang, L. C. Feldman, and W. van Saarloos, Phys. Rev. Lett. **68**, 2358 (1992).

[16]J. G. Amar, F. Family, and P.-M. Lam, in *Mechanisms of Thin Film Evolution*, edited by S. M. Yalisove, C. V. Thompson, and D. J. Eaglesham, MRS Symposia Proceedings No. 317 (Materials Research Society, Pittsburgh, 1994).

[17]G. T. Barkema, O. Biham, M. Breeman, D. O. Boerma, and G. Vidali, Surf. Sci. **306**, L569 (1994).

[18]J. A. Stroscio, D. T. Pierce, and R. A. Dragoset, Phys. Rev. Lett. **70**, 3615 (1993).

[19]E. Kopatzki, S. Gunther, W. Nichtl-Pecher, and R. J. Behm, Surf. Sci. **284**, 154 (1993).

[20]Y. W. Mo, J. Kleiner, M. B. Webb, and M. G. Lagally, Phys. Rev. Lett. **66**, 1998 (1991).

[21]H. J. Ernst, F. Fabre, and J. Lapujoulade, Phys. Rev. B **46**, 1929 (1992).

[22]W. Li, G. Vidali, and O. Biham, Phys. Rev. B **48**, 8336 (1993).

[23]R. Q. Hwang, J. Schroder, C. Gunther, and R. J. Behm, Phys. Rev. Lett. **67**, 3279 (1991); R. Q. Hwang and R. J. Behm, J. Vac. Sci. Technol. B **10**, 256 (1992).

[24]J.-K. Zuo and J. F. Wendelken, Phys. Rev. Lett. **66**, 2227 (1991).

[25]A. Brodde, G. Wilhelmi, D. Badt, H. Wengelnik, and H. Neddermeyer, J. Vac. Sci. Technol. B **9**, 920 (1991).

[26]D. D. Chambliss and R. J. Wilson, J. Vac. Sci. Technol. B **9**, 928 (1991).

[27]M. Bott, Th. Michely, and G. Comsa, Phys. Rev. Lett. **70**, 3943 (1993).

[28]Th. Michely, M. Hohage, M. Bott, and G. Comsa, Phys. Rev. Lett. **70**, 3943 (1993).

[29]C.-L. Liu and J. B. Adams, Surf. Sci. **294**, 197 (1993); **294**, 211 (1993).

[30]R. C. Nelson, T. L. Einstein, S. V. Khare, and P. J. Rous,

Surf. Sci. **295**, 462 (1993).
[31]R. Stumpf and M. Scheffler, Phys. Rev. Lett. **72**, 254 (1994).
[32]J. A. Blackman and A. Wilding, Europhys. Lett. **16**, 115 (1991).
[33]L.-H. Tang, J. Phys. (Paris) **13**, 935 (1993).
[34]M. C. Bartelt and J. W. Evans, Phys. Rev. B **46**, 12 675 (1992).
[35]J. A. Venables, Philos. Mag. **27**, 697 (1973). J. A. Venables, G. D. Spiller, and M. Hanbucken, Rep. Prog. Phys. **47**, 399 (1984).
[36]S. Stoyanov and D. Kashchiev, Curr. Topics Mater. Sci. **7**, 69 (1981).
[37]J. Villain, A. Pimpinelli, L. Tang, and D. Wolf, J. Phys. (Paris) **12**, 2107 (1992); J. Villain, A. Pimpinelli, and D. Wolf, Comments Condens. Mater. Phys. **16**, 1 (1992).
[38]A. Zangwill, in *Evolution of Surface and Thin Film Microstructure,* edited by H. A. Atwater, E. Chason, M. Grabow, and M. Lagally, MRS Symposia Proceedings No. 280 (Materials Research Society, Pittsburgh, 1992).
[39]In Ref. 32, Eq. (10) with $K_s \sim s^p$ was numerically integrated for $p \leq \frac{1}{2}$ in terms of the scaled time $\hat{t}=(DF)^{1/2}t=R^{1/2}\theta$. For $\hat{t} > 10^3$, the exponent z was within 5% of the predicted value [Eq. (19)] for all $p \leq \frac{1}{2}$. Thus, to be in the scaling regime one must have $\hat{t} > 10^3$ or $\theta > R^{-1/2} \times 10^3$. If we assume that these equations apply only in the low coverage regime $\theta < 0.01$ for which deposition on top of islands may be neglected, we have as criterion to observe exponents within 5% of the predicted value, $R > 10^{10}$.
[40]An alternative method of simulating the dynamics involves the use of a variable waiting time with a Poisson distribution between deposition or diffusion events (see Ref. 41). This method has been used in Ref. 44. However, once an average is taken over a large number of runs or a large system size, the two methods are essentially equivalent.
[41]P. A. Maksym, Semicond. Sci. Technol. **3**, 594 (1988).
[42]R. L. Schwoebel, J. Appl. Phys. **40**, 614 (1969); G. Ehrlich and F. Hudda, J. Chem. Phys. **44**, 1039 (1966).
[43]P. Stolze and J. K. Norskov, Phys. Rev. B **48**, 5607 (1993).
[44]P. Smilauer, M. R. Wilby, and D. D. Vvedensky, Phys. Rev. B **47**, 4119 (1993).
[45]R. Kunkel, B. Poelsema, L. K. Verheij, and G. Comsa, Phys. Rev. Lett. **65**, 733 (1990).
[46]Log-log plots (not shown) of monomer density N_1 versus R for different coverages θ within the intermediate regime give $\gamma = 0.671 \pm 0.006$.
[47]By measuring the shape at the beginning of the aggregation regime, Ratsch *et al.* [C. Ratsch, A. Zangwill, P. Smilauer, and D. D. Vvedensky, Phys. Rev. Lett. **72**, 3194 (1994)] estimated $\nu \simeq 0.8$ for the fractal case in this regime.
[48]S. V. Ghaisas and S. Das Sarma, Phys. Rev. B **46**, 7308 (1992). In this work the scaling of the monomer diffusion length (averaged over all coverage) was determined.
[49]A careful study of the actual rate of coalescence shows that there is already some coalescence occurring before the maximum of the island density. However, the coverage at which coalescence begins appears to increase slowly toward the maximum island density as R is increased, while the coverage corresponding to the maximum island density remains unchanged.
[50]M. C. Bartelt and J. W. Evans, Surf. Sci. **298**, 421 (1993).
[51]T. A. Witten and L. M. Sander, Phys. Rev. Lett. **47**, 1400 (1981).
[52]Substituting $k_m \sim R^{-1/6}$, Eq. (27) may be written in the form

$$S(k;R,\theta) \simeq R^{d_f/6} f_S(kR^{1/6}) f(\theta) ,$$

$$G(r;R,\theta) \simeq R^{(d_f-2)/6} f_G(r/R^{1/6}) f(\theta) .$$

[53]J. Texeira, in *On Growth and Form,* edited by H. E. Stanley and N. Ostrowsky (Martinus Nijhoff, Dordrecht, 1986).
[54]P. Jensen, A.-L. Barabaśi, H. Larralde, S. Havlin, and H. E. Stanley, Phys. Rev. E **50**, 618 (1994).
[55]S. R. Anderson and F. Family, Phys. Rev. A **38**, 4198 (1988).
[56]D. E. Sanders and J. W. Evans, Phys. Rev. A **38**, 4186 (1988).
[57]G. E. Pike and C. H. Seager, Phys. Rev. B **10**, 1421 (1974).
[58]X. Yu, P. M. Duxbury, G. Jeffers, and M. A. Dubson, Phys. Rev. B **44**, 13 163 (1991).

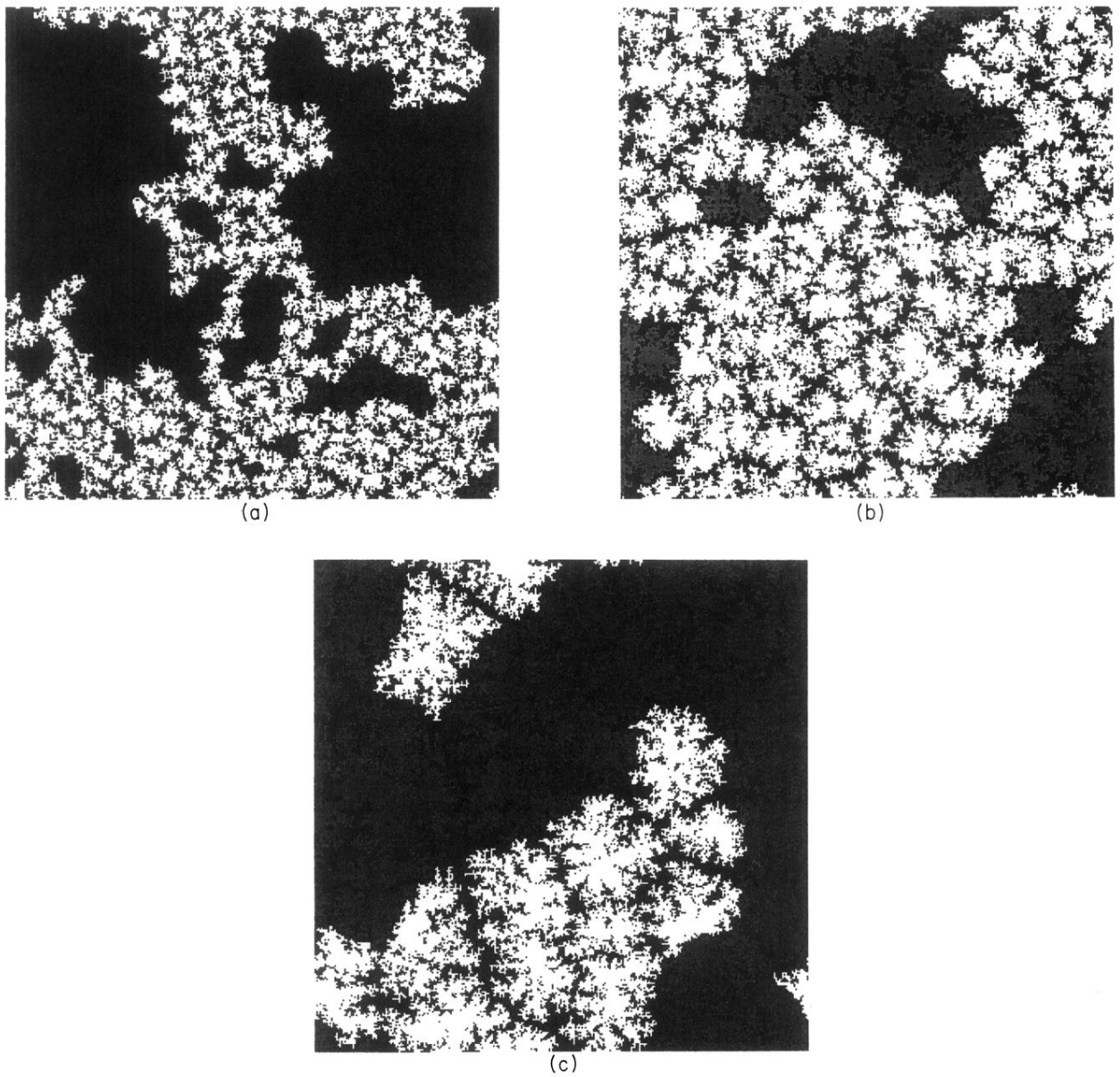

FIG. 17. Pictures of spanning cluster at percolation (white) for system size $L=300$ and large R. (a) $R=10^5$. (b) $R=10^7$. (c) $R=10^9$. Gray areas correspond to islands which are not part of the spanning cluster, while the black correspond to empty regions.

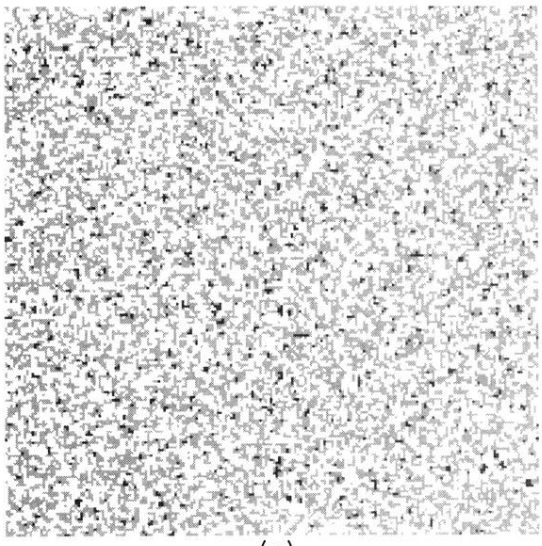

(a)

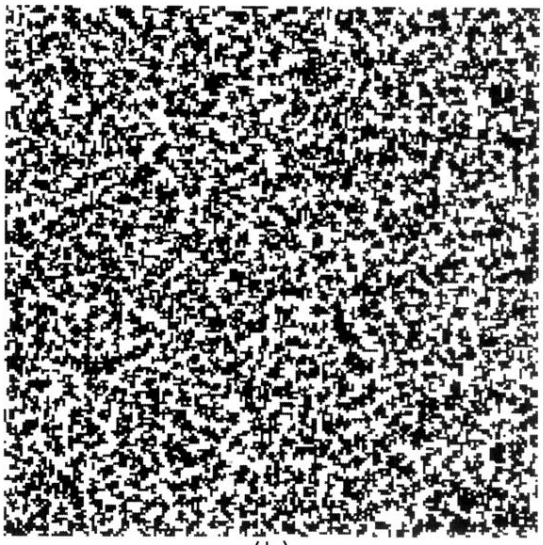

(b)

FIG. 19. (a) Gray-scale plot ($L=200$) of island morphology for $R=10^2$ and $\theta=0.5$ showing first-layer (light gray), second layer (dark gray), and some third-layer (black) growth. (b) Gray-scale plot ($L=200$) of island morphology for $R=10^3$ and $\theta=0.5$ showing first- (gray) and second-layer (black) growth.

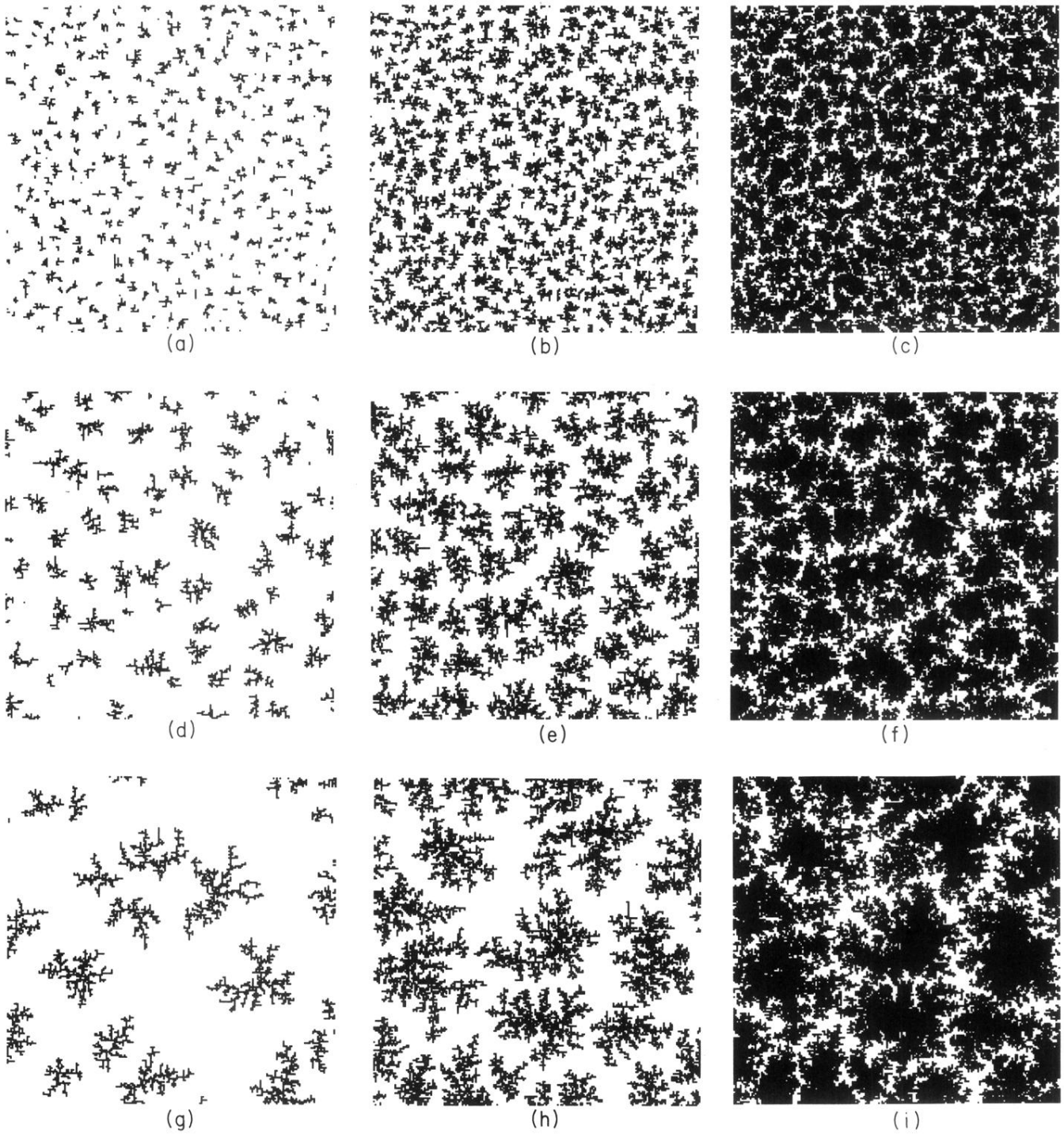

FIG. 2. Pictures of the island morphology ($L=200$) for three different values of R ($R=10^5$, 10^7, and 10^9) and three different coverages $\theta=0.1$, 0.3, and 0.7 in the beginning and middle of the aggregation regime, and in the coalescence regime. (a) $R=10^5$, $\theta=0.1$. (b) $R=10^5$, $\theta=0.3$. (c) $R=10^5$, $\theta=0.7$. (d) $R=10^7$, $\theta=0.1$. (e) $R=10^7$, $\theta=0.3$. (f) $R=10^7$, $\theta=0.7$. (g) $R=10^9$, $\theta=0.1$. (h) $R=10^9$, $\theta=0.3$. (i) $R=10^9$, $\theta=0.7$.